

**3D-PRINTED TITANIUM IMPLANTS WITH
TITANIA NANOTUBES: DUAL-SCALE
TOPOGRAPHY FOR BONE APPLICATIONS**

By CHIARA MICHELETTI, B.Eng.

A Thesis Submitted to the School of Graduate Studies in Partial Fulfilment of
the Requirements for the Degree of Master of Applied Science

McMaster University © Copyright by Chiara Micheletti, August 2018

MASTER OF APPLIED SCIENCE (2018), Materials Science and Engineering

McMaster University, Hamilton, Ontario, Canada

TITLE: 3D-printed titanium implants with titania nanotubes: dual-scale topography for bone applications

AUTHOR: Chiara Micheletti, B.Eng. (Università degli Studi di Brescia, Italy)

SUPERVISOR: Dr. Kathryn Grandfield

NUMBER OF PAGES: xv, 50

Lay Abstract

Bone implants are often made of titanium-based materials, which, despite their suitable properties, may not sufficiently bond with the living bone tissue. This can lead to implant loosening and failure. To produce customized implants, additive manufacturing, or 3D-printing, can be employed. However, these surfaces require substantial post-processing to produce features capable of promoting bone integration. In this work, a dual-scale surface topography to combine the advantages of both micro- and nanoscale roughness was created using electrochemical anodization on 3D-printed titanium alloy substrates. Preliminary physical, chemical, and biological characterizations suggest that the creation of titania nanotubes on the 3D-printed surfaces of Ti-6Al-4V and Ti-5Al-5Mo-5V-3Cr could improve their ability to bond with bone.

Abstract

Bone implants procedures involve millions of people every year worldwide. One of the main factors determining implant success is related to the ability of the prostheses to osseointegrate, i.e. to create a structural and functional connection with the living bone [1].

Titanium and titanium alloys are widely used biomaterials for bone implants, due to their superior biocompatibility and corrosion resistance, suitable mechanical properties, and natural ability to osseointegrate [2]. To further enhance the inherent tendency of this class of materials to bond with the host bone tissue, the surface of Ti-based implant is often modified to improve cell responses in terms of adhesion, proliferation and differentiation, all factors contributing to successful osseointegration. In particular, surface topography, both at the micro- and nanoscale, can enhance the implant-living bone interaction [3].

Herein, a possible surface modification strategy aimed at the creation of a dual-scale topography on two different titanium alloys, Ti-6Al-4V and Ti-5Al-5Mo-5V-3Cr, is presented. Dual-scale topography was obtained by electrochemically anodizing samples manufactured by selective laser melting to combine their intrinsic microtopography with the nanotopography offered by titanium dioxide nanotubes (TNTs) generated by anodization. Characterization of the as-printed and as-anodized samples was performed to evaluate parameters of significance in the context of osseointegration. Concerning wettability, it was observed that surfaces with TNTs exhibited high hydrophilicity. The influence of the anodization process parameters on TNTs morphology was examined, and linear dependence of the nanotube diameter on the voltage was identified. Annealing of the as-anodized samples showed that anatase was produced, while preserving the nanotube integrity. Preliminary studies to assess the bioactive properties of the samples showed the spreading of bone-like cells on these substrates and the deposition of mineral during simulated body fluid testing. Therefore, both studies provided promising results to corroborate the hypothesis that dual-scale topography could potentially improve osseointegration.

Acknowledgements

I had the incredible opportunity to join a double degree program between McMaster University (Canada) and Politecnico di Milano (Italy), an experience I will be always grateful for. The research work presented in this thesis and my year in Canada would have not been the same without contribution of the following people.

First and foremost, I would like to thank my supervisor, Dr. Kathryn Grandfield, for her invaluable guidance and support. Thank you for being a great example of the passionate interest and curiosity that move scientific research and discovery, and for showing me a new side of the engineering world.

I would also like to express my gratitude to all the members of the Grandfield Research Group, for the welcoming atmosphere I have been surrounded by since my arrival. Thank you for all the time spent together, and all the experiences we lived, from building dragons to getting addicted to card games. In particular, many thanks to Bryan, for his troubleshooting skills, all the cell culturing work, and for sharing his incredibly vast knowledge of biomaterials with me. I would like to extend a big thanks to Dakota, for the SEM sessions on the Magellan and for being my main microscopy consultant, not mentioning being the main promoter of every highly typical Canadian experience I lived. Thank you also to Ariana and Asad for their help at MARC and their contribution to this work.

A special acknowledgement to those who played a significant role in my research, especially Simon Coulson for the 3D-printing side of the project, Dr. Beth McNally for her support at MARC, and the CCEM staff for microscopy and sample preparation assistance.

I also want to sincerely thank everyone who made my year abroad so unique. To the occupants of JHE A406, because no matter the difficulties in reaching the 4th floor, the temperature swing and the fire alarm, I could have never asked for a better working environment. To my housemates, for simply being amazing and for all the hours spent chatting, which significantly contributed to broaden my (slangs) knowledge of English. Thank you to everyone who made me feel at home here in Canada.

Last but not least, my deepest gratitude goes to my family, for always being by my side, even with an ocean in between us. Everything I had the opportunity to experience and achieve in life, I owe it to you. Thank you especially for teaching me that “Roots are important in a person’s life, but people have legs, not roots, and legs are meant to make you go elsewhere”.

Table of Contents

Lay Abstract	iii
Abstract	iv
Acknowledgements	v
Table of Contents	vi
List of Figures	ix
List of Tables	xiii
List of Abbreviations	xiv
Declaration of Academic Achievement	xv
1. Introduction	1
1.1 Research motivation	1
1.2 Research objectives and hypotheses	2
2. Background	3
2.1 Bone implant materials	3
2.1.1 Biomaterial: requirements	3
2.1.1.1 Biocompatibility	3
2.1.1.2 Mechanical properties	3
2.1.1.3 Wear and corrosion resistance	4
2.1.1.4 Osseointegration	4
2.1.2 Titanium and titanium alloys	4
2.1.2.1 Titanium-bone interface	5
2.2 Additive manufacturing: selective laser melting	6
2.2.1 Characteristics and biomedical applications	6
2.2.2 Selective laser melting	7
2.2.2.1 Powder bed fusion systems	7
2.2.2.2 Process parameters and characteristics	7

2.2.2.3	Surface topography	8
2.3	Osseointegration and surface topography	10
2.3.1	Importance of the implant surface	10
2.3.2	Surface topography	10
2.3.2.1	Microscale topography	10
2.3.2.2	Nanoscale topography	11
2.3.3	Aim of surface modification and possible strategies	11
2.4	Electrochemical anodization and TiO ₂ nanotubes	13
2.4.1	Anodization process	13
2.4.2	Factors influencing nanotubes morphology	14
2.4.2.1	Electrolyte	15
2.4.2.2	Applied voltage	15
2.4.2.3	Anodization time	15
2.4.3	TiO ₂ nanotubes and surface modification of bone implants	16
3.	Materials and Methods	17
3.1	Samples manufacturing	17
3.2	Anodization	18
3.2.1	Annealing	19
3.3	Characterization	20
3.3.1	Surface characterization	20
3.3.1.1	Morphology and topography	20
3.3.1.2	Roughness	21
3.3.1.3	Wettability	21
3.3.1.4	Phase analysis	21
3.3.2	Biological characterization	21
3.3.2.1	Cell imaging	21
3.3.2.2	Bioactivity	22

4. Results	23
4.1 3D-printed samples: microscale topography	23
4.1.1 Morphology and topography	23
4.1.2 Roughness	24
4.1.3 Wettability	25
4.1.4 Cell imaging	26
4.1.5 Bioactivity	27
4.2 Anodized samples: dual-scale topography	28
4.2.1 Morphology and topography	28
4.2.1.1 Anodization at constant voltage	28
4.2.1.2 Influence of voltage on TNTs diameter	31
4.2.1.3 Influence of time on TNTs morphology	34
4.2.1.4 Anodization with initial stepwise increase of voltage	36
4.2.2 Wettability	37
4.2.3 Annealing	38
4.2.4 Cell imaging	39
4.2.5 Bioactivity	40
5. Discussion	42
6. Conclusions	45
6.1 Summary of major findings	45
6.2 Limitations and future directions	46
References	47

List of Figures

- Figure 2.1** Schematic illustration of a generic powder bed fusion system. Reproduced from [22] with permission. 8
- Figure 2.2** SEM image showing the characteristic microspherical particles arranged on the surface of a Ti-6Al-4V substrate obtained by SLM. 9
- Figure 2.3** SEM micrographs of the surface of a titanium implant subjected to laser modification to create micro- and nanoscale irregularities. A: The border between as-machined surface and laser-modified surface. B: Higher magnification of the laser-modified surface. Reproduced from [40] with permission. 12
- Figure 2.4** A: Electrochemical cell with a two-electrode set up, with platinum as the cathode and titanium as the anode. B: Reactions occurring at the Ti anode leading to the formation of an array of TiO₂ nanotubes: first a compact oxide is formed on Ti surface, then F⁻ ions in the solution start etching this layer and tubular structures are created. 14
- Figure 2.5** SEM images of (a) top side, (b) bottom side, (c) cross-section of a TNTs array obtained in an electrolyte comprised of 0.3 wt.% NH₄F and 2 vol.% H₂O in ethylene glycol at 60 V. Reproduced from [46] with permission. 15
- Figure 3.1** 2D drawing of the geometry of the samples manufactured by SLM. The area of interest (square) is coloured in blue, the holder (rectangle) in yellow. The sample were 3D-printed with a thickness (not visible in the 2D view) equal to 1 mm. 17
- Figure 3.2** Trend of the applied anodization voltage as a function of time, and inset section to better illustrate the initial stepwise increase. 19
- Figure 3.3** Example of an SEM micrograph as-acquired (left) and after a threshold was applied using ImageJ to obtain a binary image and identify the TNTs as ellipsoids (right). 21
- Figure 4.1** SEM micrographs of as-printed Ti64 (left) and Ti5553 (right) samples. In both cases, the surface is randomly covered with microspherical particles, which are characteristic of the SLM manufacturing process. 23
- Figure 4.2** Left: SEM micrograph of an as-printed Ti64 sample showing the size of some microparticles on the surface. Right: Chart of the size distribution of the microspherical particles in both Ti64 and Ti5553. Data were obtained analyzing a 350 μm x 350 μm area from a SEM micrograph per alloy and measuring 30 particles in total. 24

Figure 4.3 2D (left) and 3D (right) views of the surface of a Ti64 sample manufactured by SLM. 25

Figure 4.4 2D (left) and 3D (right) views of the surface of a Ti5553 sample manufactured by SLM. 25

Figure 4.5 SEM micrographs showing bone-like cells adhering on a 3D-printed Ti64 sample. Cells are present both in the flatter areas and stretching from the flatter regions to the microspherical particles. In particular, micrograph C shows a significantly elongated cell anchoring its filopodia onto a microsphere. 26

Figure 4.6 SEM micrographs showing bone-like cells adhering on a 3D-printed Ti5553 sample. As in case of Ti64 (Figure 4.5), cells are anchored both to the flatter areas and to the microspherical particles. In particular, a cell adhering on a microparticle is visible in micrograph C. 26

Figure 4.7 SEM image showing some precipitates on the surface of a Ti5553 sample immersed in Hanks' solution for 7 days, and its correspondent EDS analysis. Peaks relative to Ca, K, Cl and P are distinguishable in the EDS spectrum. 27

Figure 4.8 Top (left) and bottom (right) views of TNTs. Left and right images correspond to a Ti64 sample anodized for 30 minutes at 60 V and 40 V, respectively. 28

Figure 4.9 Left: Cracks visible on the surface on an anodized Ti64 sample (anodization at 60 V for 30 minutes), in particular across the microspherical particles. Right: Higher magnification image showing TNTs arrays separated by cracks on a microparticle. 29

Figure 4.10 Left: Microspherical particle on an anodized Ti64 sample (anodization at 40 V for 30 minutes) with a missing TNTs array, whose detachment may have been promoted by the presence of cracks. Right: Higher magnification image showing a side-view of the TNTs. The barrier layer, i.e. a layer of amorphous TiO₂ that forms in between the substrate and the TNTs [49], is also visible. 29

Figure 4.11 SEM image of a Ti64 sample anodized at 80 V for 30 minutes, in which it is visible how several TNTs collapsed and merged into each other forming nanograss. 30

Figure 4.12 Example of anomalous TNTs obtained by anodizing Ti5553 at 60 V for 30 minutes. Nanotubes seems to have a double wall, and extended regions of nanograss are present. 31

- Figure 4.13** SEM images of TNTs generated by anodization of Ti64 for 30 minutes at 20 V (A), 40 V (B), 60 V (C) and 80 V (D). 32
- Figure 4.14** SEM images of TNTs generated by anodization of Ti5553 for 30 minutes at 20 V (A), 40 V (B), 60 V (C) and 80 V (D). 32
- Figure 4.15** Graphs showing the variation in TNTs diameter as a function of the anodization voltage for both Ti64 and Ti5553. 34
- Figure 4.16** Morphology of TNTs on Ti64 anodized at 40 V for 5 (A), 10 (B), 20 (C) and 60 (D) minutes. 35
- Figure 4.17** Morphology of TNTs on Ti5553 anodized at 40 V for 5 (A), 10 (B), 20 (C) and 60 (D) minutes. 36
- Figure 4.18** TNTs obtained on Ti64 (left) and Ti5553 (right) by applying an initial stepwise increase of voltage. 37
- Figure 4.19** Water droplet behaviour on as-printed Ti64 (left) and after anodization at 40 V for 30 minutes (right). The anodized sample showed higher hydrophilicity, as can be inferred by the significant spreading of water (right). A similar behaviour was observed for different anodization voltages and for Ti5553 as well. 38
- Figure 4.20** TNTs on Ti64 (left) and Ti5553 (right) anodized at 40 V for 30 minutes and then annealed in open air at 500 °C for 2 hours. 38
- Figure 4.21** XRD spectrum of an anodized and annealed Ti64 sample. Peaks identified by green lines correspond to anatase. Red lines indicate titanium, most likely from the substrate underneath the TNTs film. 39
- Figure 4.22** XRD spectrum of an anodized and annealed Ti5553 sample. Peaks identified by green lines correspond to anatase. Red lines indicate titanium, most likely from the substrate underneath the TNTs film. A compound of titanium-vanadium-chromium (0.7Ti-0.1V-0.2Cr) was also detected (peaks marked by blue lines). 39
- Figure 4.23** SEM micrograph showing cell filopodia interacting with TNTs on the surface of anodized Ti64 (left) and Ti5553 (right) samples. 40
- Figure 4.24** Left: Cell on a flat area of an anodized Ti5553 sample. Right: Cell adhering both on some microparticles and on a flat region of an anodized Ti64 sample. 40

Figure 4.25 EDS spectrum and SEM image of an anodized Ti64 sample immersed in Hanks' solution for 3 days. Precipitates of Ca, P, Na and K and P are visible, and it seems that they filled the TNTs, as nanotubes pores are no longer noticeable on the surface. 41

List of Tables

Table 2.1 Mechanical properties of some titanium alloys [16]. For the sake of comparison, typical mechanical properties of bone are also included.	5
Table 4.1 Values of 2D and 3D roughness parameters of as-printed Ti64 and Ti5553 samples.	24
Table 4.2 Contact angle (CA) values measured for as-printed Ti64 and Ti5553 samples.	25
Table 4.3 Mean diameter of TNTs generated by anodization of Ti64 and Ti5553 for 30 minutes at four different voltages.	33
Table 4.4 Mean values of water contact angles (CA) obtained for both Ti64 and Ti5553 at four different anodization voltages (20, 40, 60 and 80 V).	37

List of Abbreviations

AM: additive manufacturing

CA: contact angle

ECM: extracellular matrix

EDS: energy dispersive spectroscopy

HA: hydroxyapatite

Saos-2: sarcoma osteogenic

SBF: simulated body fluid

SEM: scanning electron microscopy

SLM: selective laser melting

Ti5553: Ti-5Al-5Mo-5V-3Cr

Ti64: Ti-6Al-4V

TNT: titania nanotube

XRD: x-ray diffraction

Declaration of Academic Achievement

I hereby declare to be the sole author of this document. The research work presented in this thesis was mostly completed by myself, with the contribution of people and institutions listed below.

- 3D-printed samples of Ti64 and Ti5553 were manufactured by staff at the Additive Manufacturing Innovation Centre at Mohawk Collage (Hamilton, ON, Canada) under the direction of Simon Coulson.
- Imaging using the FEI Magellan 400 scanning electron microscope was done by Dakota Binkley.
- Cell culturing of the as-printed and as-anodized samples was carried out by Bryan Lee.
- Coating of samples prior SEM imaging was completed by staff at the Canadian Centre of Electron Microscopy at McMaster University (Hamilton, ON, Canada).
- Roughness measurements using Alicona Infinite Focus were done by associates at the McMaster Manufacturing Research Institute at McMaster University (Hamilton, ON, Canada).
- XRD characterization was carried out by staff at the McMaster Analytical X-ray Diffraction Facility at McMaster University (Hamilton, ON, Canada).

1. Introduction

1.1 Research motivation

Bones can become damaged and weakened by age, accidents or disease. When this occurs, the failed bone tissue needs to be replaced by an artificial implant, i.e. a bone implant or scaffold. A high number of implant surgeries take place: considering only the US, 1-2 million of dental implants and about 600,000 artificial hips and knees are annually implanted [4]. Moreover, the demand for bone implants is expected to continually increase in coming years due to the aging population. For example, statistics estimate that the total number of total hip replacements and knee arthroplasties will rise by 174% and 673%, respectively, by 2030 [5]. Furthermore, not only the number of initial surgeries has grown in the past years, but also that of revision surgeries, i.e. additional surgeries required in case of failure of the implant placed in the first operation.

Although the majority of bone implant procedures are successful, a non-negligible percentage of bone implants is still prone to fail, approximately 5-10% of dental implants and 7% of total joint replacements [4]. The two main causes of implant failure are aseptic loosening and infection. In regard to the former, failure is often originated by poor osseointegration, i.e. a lack of connection between the bone tissue and the implant surface [6]. Osseointegration is one of the main factors determining implant success, thus it is a paramount aspect to consider in the design of an implant (Section 2.3).

Presently, the vast majority of implants are made of metallic biomaterials [7], in particular titanium and its alloys (Section 2.1). In fact, their superior biocompatibility, high corrosion resistance and suitable mechanical properties make this class of materials ideal candidates for bone implants. Moreover, titanium shows a natural ability to osseointegrate, allowing for bone growth close to the implant surface [2]. However, implants made of titanium usually undergo some surface treatments or modifications to ensure a superior bonding to the host bone tissue and reduce the risk of implant loosening and failure [8]. In particular, it has been shown that there is a direct relationship between osseointegration and surface topography, therefore surface modification of Ti-based implants usually aims to create suitable topographical features [3]. A promising alternative is the creation of titanium dioxide nanotubes by electrochemical

anodization (Section 2.4), as nanoscale surface topography is believed to promote osseointegration [9].

1.2 Research objectives and hypotheses

The main objective of the present research was to enhance the surface properties of 3D-printed titanium alloys to create dual topography surfaces that could be more favourable for osseointegration. The specific aims of this thesis include:

1. To modify the surface of two different 3D-printed titanium alloys (Ti-6Al-4V and Ti-5Al-5Mo-5V-3Cr) by electrochemical anodization to create titanium dioxide nanotubes on microrough surfaces. The goal was to create a dual-scale surface topography by combining the microtopography of the 3D-printed samples with the nanoscale features obtained by anodization to take advantage of both micro- and nanotopography to improve cellular responses, and ultimately improve the osseointegration of Ti-based bone implants.
2. To investigate the influence of different anodization and annealing conditions on the morphology of 3D-printed substrates and resultant surfaces.
3. To perform comprehensive surface characterization to assess the potential role of the modified surfaces on osseointegration. This was achieved by analyzing morphology and topography, both before and after anodization, mainly using scanning electron microscopy, and evaluation of surface roughness and wettability. In addition, preliminary biological cell-surface interaction and bioactivity characterizations were carried out.

It was hypothesized that the substrates with a dual-scale topography would show encouraging bioactive properties in terms of cell response and mineral deposition.

2. Background

2.1 Bone implant materials

Damaged bone tissue is usually surgically substituted with an artificial replacement to restore its functionality. When designing a bone implant, selection of the right material is paramount to ensure the success of the implant itself. Requirements that need to be satisfied concern biocompatibility, high corrosion and wear resistance, suitable mechanical properties and osseointegration [10].

2.1.1 Biomaterial: requirements

2.1.1.1 Biocompatibility

Biocompatibility is a fundamental property that materials placed in contact with living tissues and organs need to exhibit. When a material is biocompatible, it can more specifically be referred to as “biomaterial”. A material is defined as biocompatible when it does not cause any harmful effects to the body [11]. When a material is implanted in the body, its interaction with body fluids, proteins and cells produces a series of reactions that determines whether or not it is accepted by the host system without causing inflammatory or allergic reactions [12]. The main issues regarding biocompatibility are thrombosis and fibrous tissue encapsulation of the implant [13]. The biomaterial surface plays a major role in determining how the body will respond to the implant, as it is the first point of contact between the implant and the host. In addition, to evaluate the overall biocompatibility of an implant, it is important to consider all the elements constituting it, since they could be released into the human body due to wear or corrosion and potentially cause adverse effects [7].

2.1.1.2 Mechanical properties

An implant material should match the mechanical properties of the tissue meant to be replaced. In case of bone, a combination of high strength and low elastic modulus is usually required. Adequate strength is fundamental for bearing the loads the implant is subjected to, specifically suitable fatigue strength to withstand repeated cyclic loading over time, thus ensuring the long-term success of the implant. Low elastic modulus is necessary as bones have a Young’s modulus varying from 4 GPa to 30 GPa, depending on the type of bone and the direction of measurement [14]. If the implant material is stiffer than bone, the majority of the load will be

carried by the implant, leaving the bone tissue unstressed. This condition is called “stress shielding effect” and leads to bone resorption around the implantation site and consequent disuse atrophy. Moreover, stiffness mismatch causes excessive relative movements between implant and bone that result in implant loosening and poor osseointegration [7].

2.1.1.3 Wear and corrosion resistance

The human body is a complex electrochemical system and it constitutes an aggressive corrosive environment for implants, as they are exposed to body fluids which carry different types of corrosive substances. When using a metallic implant, degradation products and debris produced by wear and corrosion could result in the release of metal ions, which may cause adverse effects to both the implant performance and patient health. Therefore, high corrosion and wear resistance are important characteristics for preventing the release of toxic substances and the development of infections. Furthermore, loss of implant material can result in poor implant-host tissue interaction and implant loosening [13].

2.1.1.4 Osseointegration

The ability to achieve an optimal osseointegration is a fundamental requirement for bone implants. The term *osseointegration*, coined by P.-I. Brånemark in the 1950s, refers to “a direct structural and functional connection between ordered, living bone and the surface of a load-carrying implant” [15]. To avoid its loosening, an implant must be able to integrate with the adjacent bone tissue, otherwise fibrous tissue will form at the implant-tissue interface. Implant surface plays a critical role in the achievement of good osseointegration. In this regard, fundamental surface characteristics are its chemistry, topography and roughness, as it will be discussed in Section 2.3. Although all characteristics of bone implants are important for their success, the surface features that effect osseointegration are the primary focus of this thesis.

2.1.2 Titanium and titanium alloys

Currently, 70%-80% of bone implants are made of metallic biomaterials [7], in particular titanium and its alloys (e.g. Ti-6Al-4V, a widely used Ti-based material for biomedical applications) due to their superior corrosion resistance and biocompatibility, low density, low elastic modulus and high strength [13]. Moreover, titanium shows an intrinsic ability to bond with bone, thus increasing the integration of the implant with the host tissue [2].

Elemental titanium experiences an allotropic transformation above 882.5°C from a hexagonal close packed structure, referred to as α -titanium, to a body-centered cubic structure, indicated as β -titanium [8]. In case of Ti alloys, the alloying elements contained can affect the extension of the α - or β -phase field or promote the formation of a two-phase $\alpha+\beta$ field. Therefore, four categories of titanium alloys can be distinguished, i.e. α , near- α , $\alpha+\beta$, metastable β , or β alloys. Presently, there is an increasing interest in the use of β alloys for bone implants, as they show higher strength and lower modulus compared to α and $\alpha+\beta$ alloys [7]. In fact, although Ti and its alloys have an elastic modulus closer to that of bone than other metallic biomaterials, the stiffness mismatch can still result in stress-shielding. Mechanical properties of some titanium alloys of interest are collected in Table 2.1.

Table 2.1 Mechanical properties of some titanium alloys [16]. For the sake of comparison, typical mechanical properties of bone are also included.

Material	Microstructure	E [GPa]	σ_y [MPa]	UTS [MPa]
Pure Ti (grade 1 to 4)	α	102.7-104.1	170-485	240-550
Ti-6Al-4V	$\alpha+\beta$	110-114	825-869	895-930
Ti-6Al-7Nb	$\alpha+\beta$	114	880-950	900-1050
Ti-5Al-2.5Fe	$\alpha+\beta$	112	895	1020
Ti-12Mo-6Zr-2Fe (TMZF)	β	74-85	1000-1060	1060-1100
Ti-13Nb-13Zr	β	79-84	836-908	973-1037
Ti-29Nb-13Ta-4.6Zr	β	80	864	911
Bone [17]	/	10-30	/	90-140

2.1.2.1 Titanium-bone interface

The superior biocompatibility of titanium is mainly due to the passive oxide layer that spontaneously forms on its surface when in contact with air or aqueous environments. This oxide is highly stable and compact, and immediately rebuilds when damaged. It is normally a few nanometers thick (2-5 nm) and it mainly consists of amorphous titanium dioxide [18]. The passive film is stable in biological environments over long periods of time, provides high corrosion resistance and slows down the transmission of undesirable ions. In addition, it is bioinert, thus it does not react with body fluids and tissues and does not cause adverse reactions. Although titanium shows a natural ability to integrate with bone [2], TiO₂ inertness can hinder the formation of bonds with bone cells, which in turn may lead to the development of fibrous tissue around the implant. Therefore, titanium implants usually undergo surface treatments, so that better and more rapid bonding to bone can be achieved [8].

2.2 Additive manufacturing: selective laser melting

2.2.1 Characteristics and biomedical applications

Additive manufacturing (AM), sometimes also called rapid prototyping or 3D-printing, refers to a group of technologies that, in contrast to traditional subtractive methods, fabricate components from the bottom-up by adding material one layer at a time [19]. ASTM international defines AM as the “process of joining materials to make objects from 3D model data, usually layer upon layer, as opposed to subtractive manufacturing methodologies”¹. The AM process starts with a 3D model of the part to be realized, usually created using a computer-aided design (CAD) software. The 3D CAD model is then converted in a .STL file and sliced into cross-sectional layers by a specialized software. The data set generated is then sent to the AM machine which creates the object layer by layer selectively placing or forming the material. This process is often compared to an inkjet printer, and this is why AM is sometimes referred to as “3D-printing” [19].

The main advantage of AM is the great control over the part design, as it enables creation of physical components directly from a digital file [19]. Moreover, it is possible to manufacture parts with a level of complexity not achievable with other processes, and complex features can be realized even in a single step [20]. Furthermore, the process is economically sustainable also in case of small batches, even a single component, which is beneficial to better fulfill the customer’s demand. Compared to conventional techniques, AM also shows a higher efficiency in material use, as the excess material can be often reused, and in the use of resources, since conventional processes often requires multiple auxiliary resources other than the main primary machine tool. On the other hand, AM processes are quite limited in regard to mass production and obtainment of large objects. In addition, AM parts often show rough and ribbed surfaces, thus additional steps are necessary when a better surface finish is required [20].

AM is suitable for producing components in several fields, including parts for biomedical applications. As already mentioned, this process shows superior flexibility compared to conventional techniques, as it makes it possible to manufacture complex geometries and highly

¹ Standard Terminology for Additive Manufacturing Technologies, ASTM F2792-10, June 2010.

customized parts [21]. Therefore, it is possible to produce patient-specific and one-of-a-kind devices avoiding the high costs associated to traditional processes. Furthermore, some AM techniques can be employed with biocompatible metals, such as titanium and its alloys, which are sometimes difficult and expensive to machine in a traditional way [22]. Finally, AM offers control over porosity and surface topography, which are fundamental aspects in different biomedical applications.

2.2.2 Selective laser melting

2.2.2.1 Powder bed fusion systems

Selective laser melting (SLM), sometimes also indicated as direct metal laser sintering, is an evolution of the older selective laser sintering process, which gave origin to the broader category of powder bed fusion technologies. A generic powder bed system is shown in Figure 2.1. It consists of a laser scanning system, a powder delivery system, a roller and a fabrication piston. The laser beam can be substituted with an electron beam, resulting in the technique called electron beam melting. The process is usually carried out in a build chamber under a protective/inert atmosphere, using gases such as Ar or N₂. It starts lowering the fabrication piston and moving up the powder delivery piston by one-layer thickness. The powder is spread across the working area and slightly compressed with a roller. In particular, the first layer of powders is deposited onto a base plate, that provides better anchoring of the part during its manufacturing [20]. Afterwards, the energy source, either a laser or an electron beam, is scanned over the powder bed to selectively sinter and/or melt the powder to realize a cross-sectional layer of the 3D model. Upon completion of a layer, the fabrication piston is lowered by another layer thickness and a new layer of powder is raked. The process is repeated until the obtainment of the final 3D object, which is usually made of hundreds or even thousands of layers [20].

2.2.2.2 Process parameters and characteristics

The working principle of the SLM technique is that described previously for a generic powder bed fusion system. This technique is mainly controlled by parameters such as laser power, powder layer thickness, scanning speed and scan line spacing [20]. The process parameters are usually optimized to achieve the highest density, and this often enables to obtain components with mechanical properties comparable or even superior to the correspondent conventionally manufactured parts. This is one of the unique advantages of SLM. Another benefit is that SLM

makes it possible to manufacture complex geometries and highly customizable parts, which is an aspect of great interest in case of biomedical applications. Moreover, SLM can be employed with several metals and their mixtures, so it can be used to manipulate already existing alloys or to develop new ones. Furthermore, waste of material is negligible, since the excess powders can be reused after proper treatment [20].

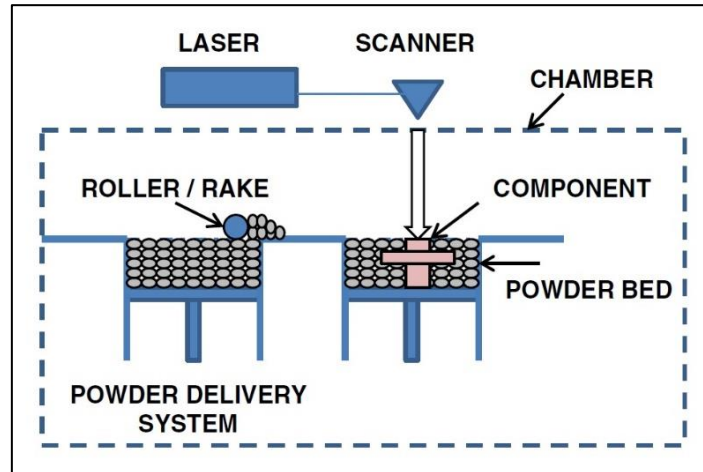


Figure 2.1 Schematic illustration of a generic powder bed fusion system. Reproduced from [23] with permission.

2.2.2.3 Surface topography

As it will be discussed in more detail in Section 2.3, surface topography has been shown to play a major role concerning osseointegration of bone implants, as macro-, micro- and nanoscale features influence cell adhesion, proliferation, and migration [24].

Surface topography of parts obtained by SLM is characterized by the presence of randomly distributed microspherical particles, as shown in Figure 2.2. These particles, whose size and morphology are similar to those of the feedstock powders, are attributed to non-fully melted particles sintered at the surface and to the balling effect [25]. The former effect occurs when the energy input is insufficient, thus some particles do not completely melt but they sinter at the surface instead [26]. Balling, instead, is caused by splashes of molten material due to the high capillary instability of the melt [27].

The presence of these microspherical particles on the surface of SLM parts results in a surface topography with a roughness in the microscale range. While such microrough surfaces are detrimental for some applications, where a higher surface finish is required, such substrates are believed to be beneficial in case of bone implants, as cells are sensitive to microtopography

(Section 2.3.2.1) [28], [29]. However, the presence of microparticles can be deleterious if they detach from the substrate and they are released in the biological system, as they may result in adverse responses and inflammation.

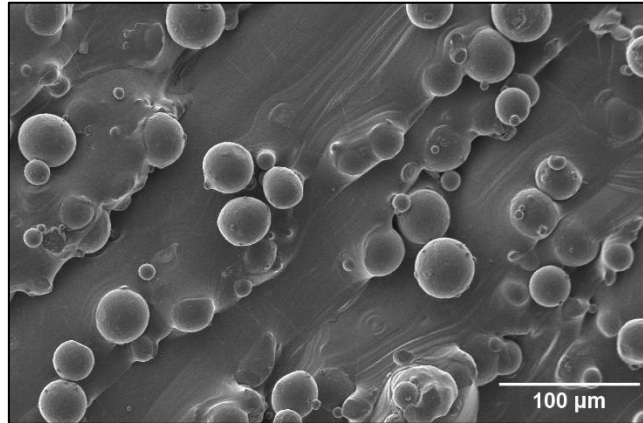


Figure 2.2 SEM image showing the characteristic microspherical particles arranged on the surface of a Ti-6Al-4V substrate obtained by SLM.

2.3 Osseointegration and surface topography

2.3.1 Importance of the implant surface

While bulk properties, such as mechanical strength, determine the suitability of a biomaterial to be used as a bone implant, the surface is where interaction with the biological environment occurs. Therefore, implant surface influences cell adhesion, migration, proliferation and differentiation. Tailoring surface properties can enhance cellular responses and new bone formation, in turn improving osseointegration [30]. In fact, if the properties are not adequate, cell colonization on the implant surface can result in the formation of a layer of fibrous tissue that hinders proper interaction between the implant itself and bone, resulting in implant loosening and failure [31].

Albrektsson and Wennerberg [32] identified three main categories of implant surface quality, i.e. mechanical properties, topographic properties, and physicochemical properties. They also pointed out that all these properties are interconnected, and by changing one, also those in the other two groups will be affected. Chemical and physical parameters are often interrelated, and it is sometimes difficult to characterize them separately and decouple the respective role on biological systems [9]. This is particularly relevant at the nanoscale, as surface nanotopography usually induces some changes also in the chemistry [33].

2.3.2 Surface topography

The existence of a direct relationship between surface topography and osseointegration has been widely demonstrated in literature [1], [34], [35]. When designing an implant, its macroshape is important for having an optimal primary fixation, but surface characteristics at lower length scales, namely micro-, submicro- and nanoscale, are also to be considered to achieve a successful and long-term osseointegration. The terms to micro-, sub-micro and nanoscale usually refers to features having at least one of their dimensions (height, length or width) smaller than 100 μm , 1 μm and 100 nm, respectively [31].

2.3.2.1 Microscale topography

Several authors agree on the role played by microscale topography, usually in the range 1-10 μm , in improving bone formation [3]. Three main theories have been developed to explain

how microtopography can increase bone-implant contact. Hansson and Norton [36] developed a biomechanical hypothesis, highlighting how microtopography can increase the contact surface between bone and implant and thus their mechanical interlock, which in turns is important for osseointegration. Davies [37] proved the importance of topography at the microscale on enhancing contact osteogenesis, i.e. new bone formation on the implant surface, and osteoconduction, i.e. the ability of a surface to permit bone growth on it [38]. The third hypothesis concerns the influence of surface topography on signaling and cell behaviour, as many *in vitro* investigations have observed a range of microroughness that seems improving osteoblast (bone-forming cells [39]) adhesion and extracellular matrix (ECM) deposition and mineralization [1].

2.3.2.2 Nanoscale topography

While the importance of microscale topography for higher osseointegration has been widely recognized, the mechanisms by which nanotopography can contribute to osseointegration are still not so clear [9]. As already mentioned, one of the main problems is to distinguish the influence of topography from that of chemistry, as nanomodification of implant surface may affect both these aspects [33]. In general, nanoscale topography seems to affect cell interactions with a surface and cell behaviour. One reason is that, at the nanoscale, a more complex topography increases the surface energy, and this changes the ECM protein adsorption on the surface, which in turns control cell adhesion [9]. Moreover, it is believed that nanopatterning can influence cell proliferation and differentiation, mainly because it mimics the nanoscale features typical of the natural environment where cells are embedded, namely the ECM [40].

2.3.3 Aim of surface modification and possible strategies

Implant surface is usually modified to improve its capacity to create an optimal interface with bone, in turn enhancing osseointegration. Among the possible approaches, given the relationship between surface topography and osseointegration, alterations in surface structure both at the micro- and nanoscale are commonly performed to improve cell responses. For example, different methods are currently used for increasing the roughness of clinically-employed Ti implants. Some of these techniques consist in blasting, abrading, coating, chemical etching in order to create surface features with different forms, shapes and sizes, aimed to improve cell responses [35]. An emerging technique employs laser as a micromachining tool to produce complex surface geometries both at micrometre, sub-

micrometer and nanometre level (Figure 2.3) [41]. For what concerns bone implants clinically in use, plasma-sprayed hydroxyapatite coatings are the most adopted solution. This type of coating is advantageous not only for its roughness and porosity, but also for its bioactivity [42].

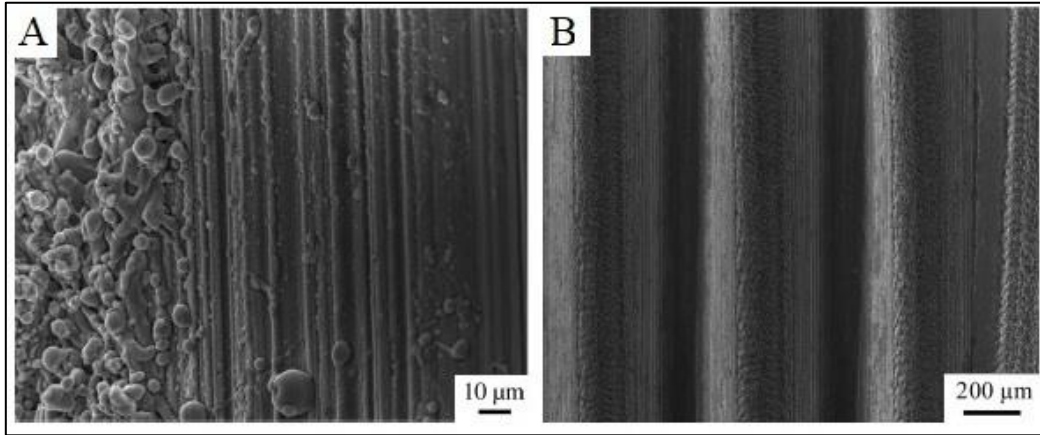


Figure 2.3 SEM micrographs of the surface of a titanium implant subjected to laser modification to create micro- and nanoscale irregularities. A: The border between as-machined surface and laser-modified surface. B: Higher magnification of the laser-modified surface. Reproduced from [41] with permission.

2.4 Electrochemical anodization and TiO₂ nanotubes

A layer of titanium dioxide nanotubes with a controlled and uniform diameter can be produced by electrochemical anodic oxidation, which is a simple, versatile and cost-effective surface treatment for metallic implants. Metals like titanium, aluminum, niobium, zirconium and tantalum, also known as “valve metals”, spontaneously form an ordered nanoporous oxide layer when used as the anode of an electrochemical cell, if parameters like voltage, current and electrolyte properties are properly selected [18]. The presence of TNTs on Ti-based implant surface can improve their biocompatibility, enhance osseointegration thanks to the creation of a nanoscale topography, and reduce the risk of infections if the nanotubes are employed as a local drug delivery system [43].

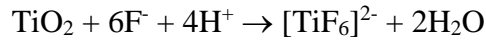
2.4.1 Anodization process

The anodization process is performed in an electrochemical cell either with a two- or three-electrode configuration [18]. In a two-electrode set-up (Figure 2.4A), the metallic substrate of interest is employed as the working electrode (anode) and it is immersed in an electrolyte with a counter-electrode (cathode). The process starts when an external voltage is applied between anode and cathode, and it usually carried out maintaining the voltage constant [44]. Depending on the anodization parameters and the electrolyte used, three main reactions can occur in the electrochemical cell: dissolution of the metal and formation of metal ions that dissolve in the solution, interaction of metal ions with oxygen ions in the electrolyte to form metal oxide, which can be deposited as a bulk coating on the anode, or formation of a porous metal oxide layer if specific conditions lead to a competition between oxide formation and dissolution. In regard to this last case, such conditions can be obtained using a fluoride-based electrolyte. In case of titanium anodes, this makes it possible to fabricate well-aligned nanotubular structures, i.e. TNTs [44].

The mechanism of nanotubes formation can be summarized in four steps, schematically illustrated in Figure 2.4B [44]. First of all, a thin compact layer of TiO₂ is formed on the anode surface, according to the reaction:



Secondly, small cracks start forming in the oxide layer, mainly due to the applied voltage. The electrolyte starts flowing into these cracks, promoting the dissolution of TiO_2 layer and the formation of the soluble compound $[\text{TiF}_6]^{2-}$:



The third step involves the expansion of these small cracks that start merging with neighbouring cracks resulting in the formation of pores. At this point, the fluoride ions' continuous attack inside the pores of the oxide leads to pore growth and ultimately the creation of parallel tubular structures. Such tubes usually have a V-shape, with thinner walls at the top than at the bottom, as the dissolution action of fluoride ions is higher at the top due to the increased content in proximity of the electrolyte.

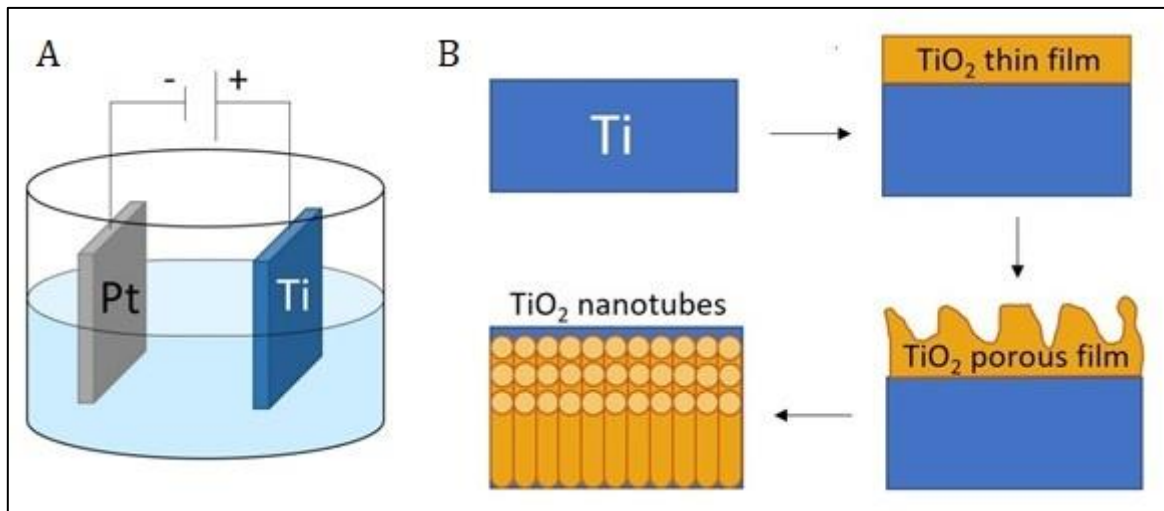


Figure 2.4 A: Electrochemical cell with a two-electrode set up, with platinum as the cathode and titanium as the anode. B: Reactions occurring at the Ti anode leading to the formation of an array of TiO_2 nanotubes: first a compact oxide is formed on Ti surface, then F^- ions in the solution start etching this layer and tubular structures are created.

2.4.2 Factors influencing nanotubes morphology

One of the main advantages of the anodization process is the control over the nanotubes morphology, i.e. diameter and length, by varying process parameters and/or electrolyte characteristics. Creation of the nanotubes relies on the competition between formation and dissolution of the TiO_2 layer, and the interplay of these two reactions determines tube length and diameter [44].

2.4.2.1 Electrolyte

Different types of substances can be employed as electrolytes for anodizing titanium, such as acids, alkaline or natural salts solutions. TiO₂ nanotubes are created when using fluoride-based electrolytes, but some recent developments in the process have led to the synthesis of nanotubes even in fluoride-free solutions [45]. Some electrolytes commonly employed consist of polar organic solvents, such as ethylene glycol, used together with a fluoride-containing species, for example ammonium fluoride. In general, chemical dissolution and F⁻ ions transmission is relatively low in organic electrolytes, so nanotubes formed in these conditions are usually more homogeneous but may be partially covered with a hazy layer [46]. Ethylene glycol-based solutions have been used to synthesize TNTs at anodization voltages ranging from 20 to 65 V, together with a content of ammonium fluoride usually ranging 0.1 to 0.5 wt.% and 1 to 4 vol.% of water [45]. An example of nanotubes obtained using this type of electrolyte is shown in Figure 2.5.

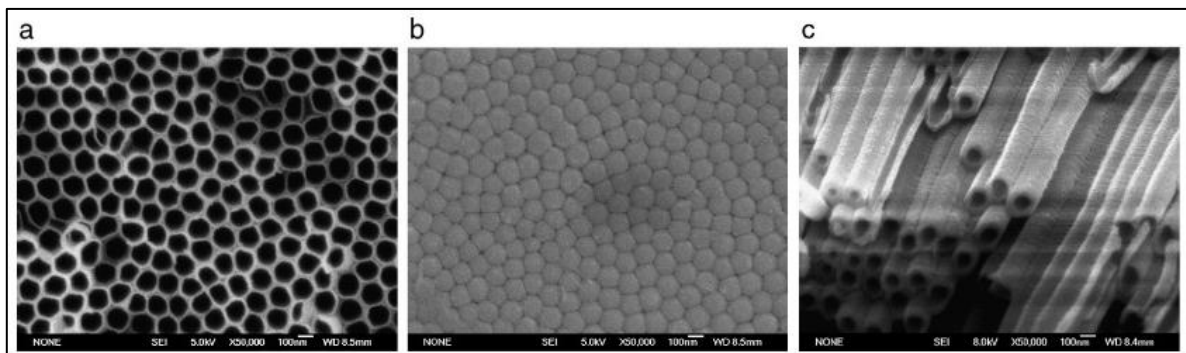


Figure 2.5 SEM images of (a) top side, (b) bottom side, (c) cross-section of a TNTs array obtained in an electrolyte comprised of 0.3 wt.% NH₄F and 2 vol.% H₂O in ethylene glycol at 60 V. Reproduced from [47] with permission.

2.4.2.2 Applied voltage

The applied voltage mainly controls the nanotubes diameter. Specifically, the diameter increases by increasing the voltage. In fact, by increasing the voltage, the movement of ions increases, thus enhancing the transmission of the ions over the oxide layer, accelerating the electrochemical etching speed [44].

2.4.2.3 Anodization time

The length of the nanotubes array increases by increasing the anodizing time, as the thickness of the oxide layer grows with time. However, at a certain point a balance between oxidation and dissolution of TiO₂ is reached, thus the tube length becomes independent on the synthesis time. In general, more regular nanotubes are formed with a shorter anodization time, while for

long processes the structure starts to be more irregular, mainly because of the excessive dissolution along the entire tube length [44].

2.4.3 TiO₂ nanotubes and surface modification of bone implants

Electrochemical anodization of titanium has recently grown in interest as a surface modification technique for Ti-based bone implants to promote osteogenesis, osteoconduction and osseointegration [48]. Advantages of TNTs coatings on bone implants include their excellent chemical inertness and therefore biocompatibility, high surface area, mechanical robustness, and surface chemistry [49], in particular wettability [50].

Studies in literature have shown that anodic TNTs can enhance cell adhesion and function, accelerate the growth kinetics of hydroxyapatite, and influence bone formation and development [51]. Despite the fact that the majority of these results have been obtained in *in vitro* studies, similar conclusions have been reached in a few *in vivo* investigations [48].

An interesting aspect is the effect of the nanotube size on cell responses. As cells are sensitive to topographical cues, electrochemical anodization appears to be a facile approach to obtain surfaces with specific surface features by controlling the nanotubes diameter. This process, in fact, can be used to synthesize nanotubes with diameters ranging to virtually any value between 10 and 250 nm [52]. Moreover, the self-ordering nature of the TNTs array makes it possible to obtain this type of coating even on complex shaped surfaces, such as screws, plates, nails and wires [49]. Several studies have shown that the tube diameter influences cell adhesion, proliferation, and differentiation. Different authors have also found that nanotubes with a diameter around 15 nm show particularly encouraging results for what concerns enhancement of cell responses [52]. Therefore, anodization of titanium to create TNTs seems to be a promising strategy of surface modification of bone implants to create a nanoscale topography, which is believed to be beneficial for osseointegration (Section 2.3).

Moreover, Gulati et al. [28] and Maher et al. [29] have investigated the possibility of producing TNTs on 3D-printed microrough samples. In this way it would be possible to obtain surfaces with a dual-scale topography, combining the microscale from the 3D-printed substrates with the nanoscale of the anodic nanotubes. This dual topography may be beneficial for combining the advantages of both micro- and nanotopography in order to improve osseointegration.

3. Materials and Methods

3.1 Samples manufacturing

3D-printed samples of two different titanium alloys, i.e. Ti-6Al-4V (abbr. Ti64) and Ti-5Al-5Mo-5V-3Cr (abbr. Ti5553) were manufactured by selective laser melting using a direct metal laser sintering system (EOSINT M 280 by EOS). Powders employed (purchased from AP&C) had a particle size of 15-45 μm and 25-63 μm for Ti64 and Ti5553, respectively. Layer thickness used for printing was equal to 60 μm . The samples were manufactured according to the geometry illustrated in Figure 3.1. This geometry was designed so that the square portion (10 mm x 10 mm), constituting the area of interest, could be handled using the rectangular part (10 mm x 3 mm). After manipulation, the rectangular portion of the specimen was easily removed. This sample design resulted to be convenient for the anodization process further explained in Section 3.2. To remove manufacturing debris, the samples were sonicated in ethanol, acetone and deionized water for 15, 15 and 5 minutes, respectively.

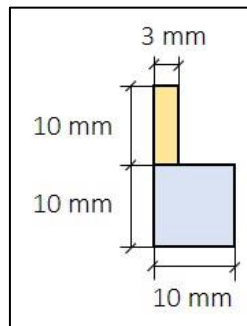


Figure 3.1 2D drawing of the geometry of the samples manufactured by SLM. The area of interest (square) is coloured in blue, the holder (rectangle) in yellow. The sample were 3D-printed with a thickness (not visible in the 2D view) equal to 1 mm.

3.2 Anodization

Electrochemical anodization was employed to generate TNTs on 3D-printed Ti64 and Ti5553 samples. A two-electrode set-up was used, with a platinum foil (25 mm x 25 mm x 0.125-0.135 mm, Sigma Aldrich) as the counter-electrode. The platinum foil (cathode) and the 3D-printed sample (anode) were connected to a power supply using alligator clips. The clips were placed onto the rectangular portion of the 3D-printed samples (Figure 3.1). Anode and cathode were then immersed into the electrolyte solution, such that only the square part of the 3D-printed sample was immersed in the solution to avoid contamination from the alligator clips and alteration of expected electrochemical reactions.

A solution of ethylene glycol (certified grade, Fisher Chemical) with 0.3 wt.% of ammonium fluoride (certified ACS grade, Fisher Chemical) and 2 vol.% of deionized water was used as electrolyte. The solution was magnetically stirred for 20 minutes before usage to ensure that it was homogeneous.

Anodization was carried out using different time and voltage conditions. To evaluate the effect of the voltage on the nanotubes morphology, samples were anodized at a constant voltage of 20 V, 40 V, 60 V and 80 V for 30 minutes. The influence of time was assessed by applying a constant voltage of 40 V and anodizing for 5, 10, 20 and 60 minutes. Finally, some samples were anodized by initially increasing the voltage in a stepwise way, as illustrated in Figure 3.2. Starting from 6 V (due to limitations of the power supply used), the voltage was then augmented by 1 V every 10 seconds until reaching 40 V; such voltage was then maintained constant for 30 minutes to complete the anodization process.

In all cases, the electrolyte was slightly magnetically stirred during the whole process. Fresh solution was used every time. After anodization, the samples were rinsed with ethanol and deionized water and sonicated in ethanol for 30 seconds.

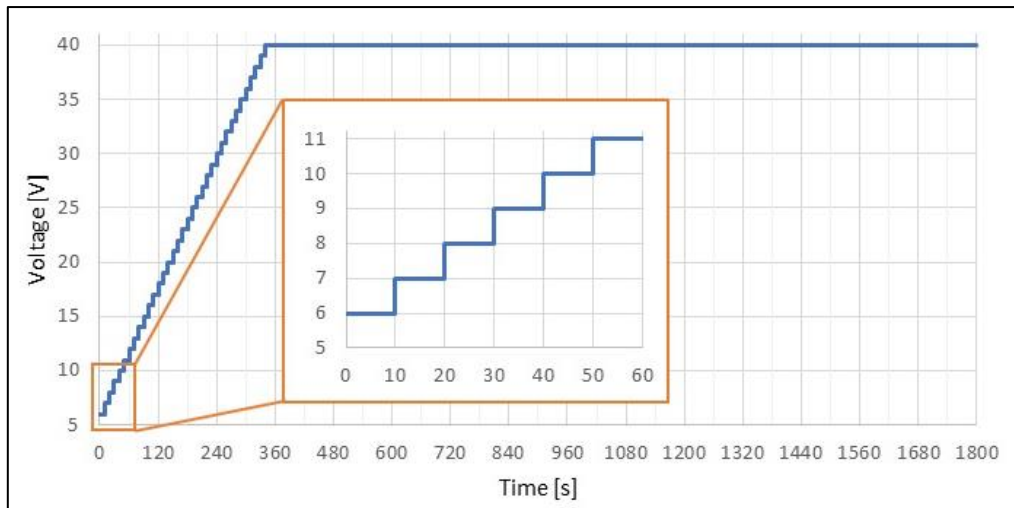


Figure 3.2 Trend of the applied anodization voltage as a function of time, and inset section to better illustrate the initial stepwise increase.

3.2.1 Annealing

As-anodized TNTs are usually made of amorphous titanium dioxide. However, it is possible to perform a subsequent annealing treatment to make TiO_2 crystallize, usually obtaining rutile and/or anatase, depending on the conditions adopted. Ti64 and Ti5553 samples anodized at 40 V for 30 minutes were annealed in open air at 500 °C for two hours.

3.3 Characterization

3.3.1 Surface characterization

3.3.1.1 Morphology and topography

Scanning electron microscopy (SEM) is the gold standard for morphological and topographical characterization at the micrometre and nanometre level [53]. Samples as printed, anodized and annealed were imaged by SEM using two different instruments, JEOL JSM-7000F and FEI Magellan 400. Before imaging, samples were mounted on a stub with carbon tape and grounded using nickel paint to reduce charging effects. Secondary electron images were acquired with acceleration voltages of 2-3 kV.

The diameter of TNTs obtained using different anodization conditions was measured using ImageJ. A threshold was first applied to each SEM micrograph to generate a “binary”, black and white, image, in which nanotubes appeared as ellipses, as shown in the example in Figure 3.3. In this way it was possible to process each image using the “Analyze Particles” command, which allowed to measure the major and minor axes of each TNT ellipsoid. Finally, the nanotube diameter was computed as the average of the dimension of major and minor axes. For each SEM image, the diameter of tens to hundreds of TNTs was measured, and the mean of all the values was used to represent the nanotube diameter of an entire image. For each anodization condition, two SEM micrographs were analyzed, i.e. one for a flatter region of the sample surface and the other for the top of a microspherical particle. The representative diameters of both images were then averaged to obtain the TNTs diameter corresponding to each anodization condition under investigation. Finally, Student’s *t*-test was used to verify if eventual differences between different groups of samples were statistically significant (significance level of $\alpha = 0.05$).

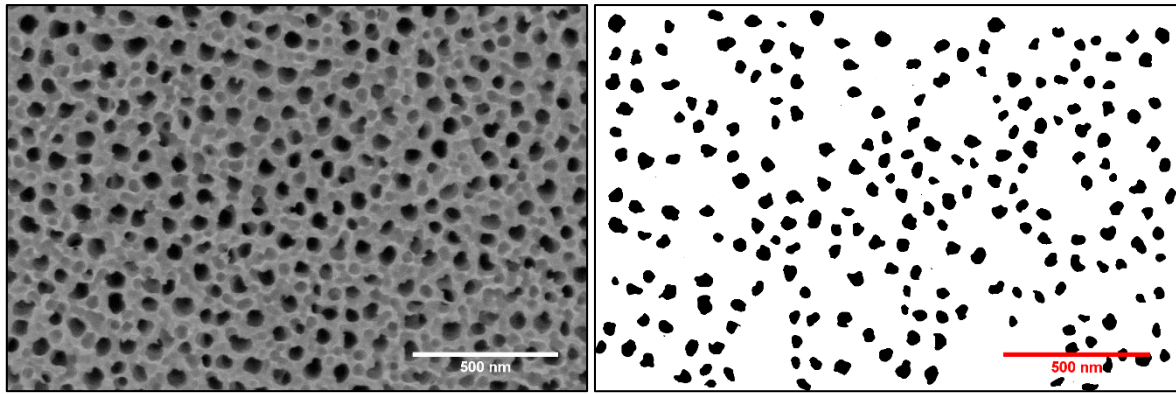


Figure 3.3 Example of an SEM micrograph as-acquired (left) and after a threshold was applied using ImageJ to obtain a binary image and identify the TNTs as ellipsoids (right).

3.3.1.2 Roughness

Roughness of the 3D-printed samples was measured by focus variation (Alicona Infinite Focus), which is a non-contact optical technique for roughness evaluation [54]. Two-dimensional and three-dimensional reconstructed views of the surface were acquired. Both profile and surface roughness parameters were measured. Measurements were done in triplicates and statistically averaged.

3.3.1.3 Wettability

Wettability was evaluated using a contact angle measuring device (DataPhysics Optical Contact Angle, OCA 35). Values of the contact angle were assessed for the samples as printed and for the samples anodized at constant voltage for 30 minutes. In both cases, measurements were done in triplicates and then statistically averaged.

3.3.1.4 Phase analysis

X-ray diffraction (XRD) was used to identify the crystalline phases of the TiO₂ nanotubes array after annealing, in order to assess whether the treatment succeeded in the creation of anatase and/or rutile. Measurements were obtained by an x-ray diffractometer with Co K α radiation (Bruker Discover D8).

3.3.2 Biological characterization

3.3.2.1 Cell imaging

Sarcoma osteogenic (Saos-2) bone-like cells were cultured on Ti64 and Ti5553 samples both as-printed and anodized at 40 V for 30 minutes. After 1 day, cells grown on the samples were fixed by glutaraldehyde and stained with osmium tetroxide. Successively, the samples were

dehydrated using increasingly concentrated solutions of ethanol and dried by critical point drying. Finally, they were coated with platinum (10 nm) before SEM imaging.

3.3.2.2 Bioactivity

Bioactivity was tested for both Ti64 and Ti5553 using three different groups of samples, i.e. as-printed, anodized at 40 V for 30 minutes, and annealed after anodization. Samples were immersed for 3 and 7 days in 25 ml of simulated body fluid (SBF) Hanks' solution (Hanks' balanced salts solution without sodium bicarbonate, Sigma-Aldrich) and stored at 37 °C. Following immersion, the samples were removed from the solution, rinsed with deionized water and let dry in air. SEM and EDS were used to verify the eventual presence of precipitates, in particular hydroxyapatite (HA) crystals, on the surface.

4. Results

4.1 3D-printed samples: microscale topography

4.1.1 Morphology and topography

SLM was used to manufacture Ti64 and Ti5553 samples, representative of possible bone implant substrates. This technique was selected to produce samples with a microscale surface topography. Such objective was reached for both the alloys employed, as assessed by SEM imaging of the as-printed samples. In fact, as shown in Figure 4.1, SEM revealed the presence of microspherical particles randomly distributed on the surface, which was the expected outcome of SLM. As shown in the chart in Figure 4.2, the microparticles visible on the surface were different in size, with diameters approximately ranging from 5 μm to 50 μm , and a mean diameter around 27 μm .

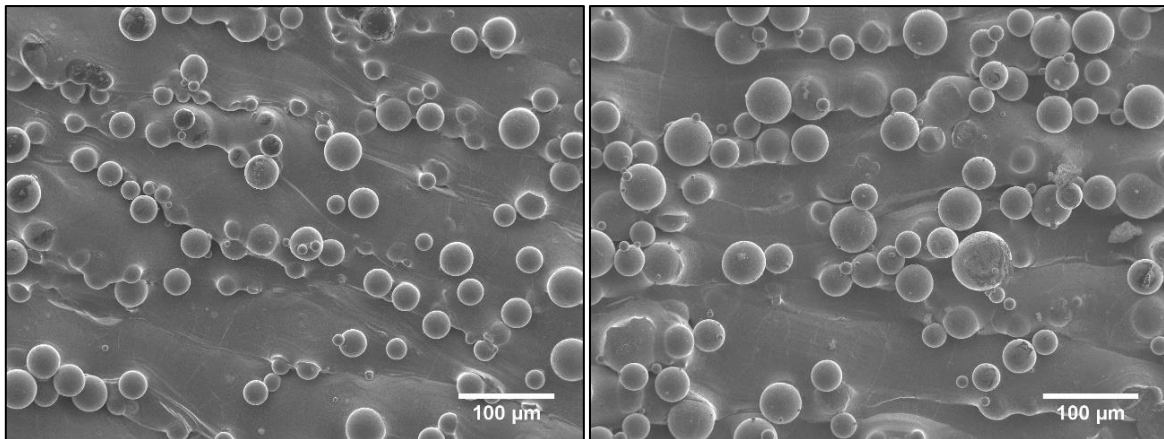


Figure 4.1 SEM micrographs of as-printed Ti64 (left) and Ti5553 (right) samples. In both cases, the surface is randomly covered with microspherical particles, which are characteristic of the SLM manufacturing process.

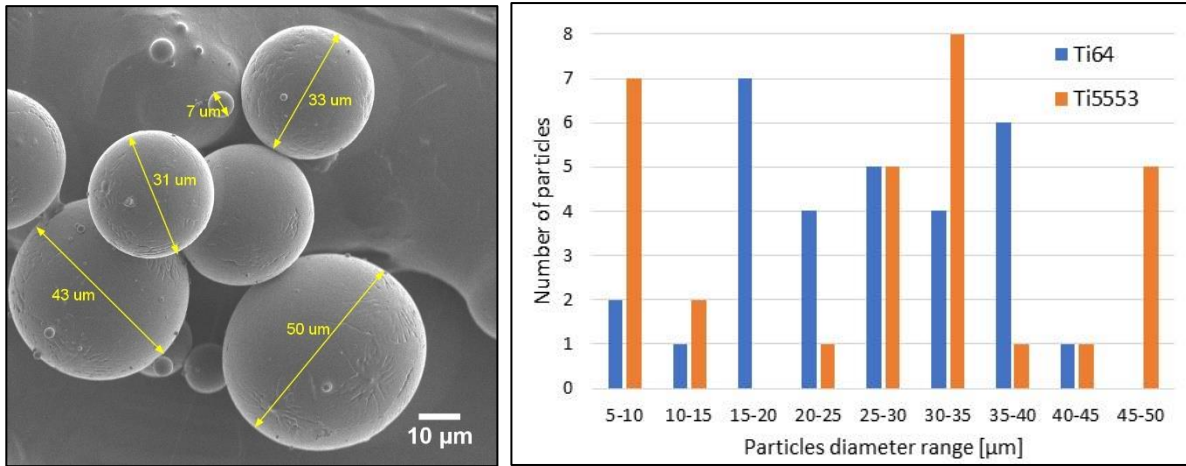


Figure 4.2 Left: SEM micrograph of an as-printed Ti64 sample showing the size of some microparticles on the surface. Right: Chart of the size distribution of the microspherical particles in both Ti64 and Ti5553. Data were obtained analyzing a 350 μm x 350 μm area from a SEM micrograph per alloy and measuring 30 particles in total.

4.1.2 Roughness

Values of roughness parameters measured by focus variation are reported in Table 4.1. Figure 4.3 and Figure 4.4 show 2D and 3D reconstructed views of the substrates for Ti64 and Ti5553, respectively. Both as-printed Ti64 and Ti5553 samples proved to have microrough surfaces, as the roughness parameters measured all laid in the microscale range. The two alloys had comparable roughness: mean values of arithmetic roughness (R_a), for example, were around 13.0 μm and 15.6 μm for Ti64 and Ti5553, respectively.

Table 4.1 Values of 2D and 3D roughness parameters of as-printed Ti64 and Ti5553 samples.

		Ti64	Ti5553
2D roughness parameters	R_a [μm]	13.0 ± 3.0	15.6 ± 1.7
	R_q [μm]	15.6 ± 3.6	19.1 ± 2.2
	R_z [μm]	48.4 ± 10.1	56.6 ± 4.6
3D roughness parameters	S_a [μm]	14.3 ± 1.2	16.9 ± 0.3
	S_q [μm]	17.5 ± 1.4	21.0 ± 0.1
	S_z [μm]	125.1 ± 9.9	152.9 ± 4.5

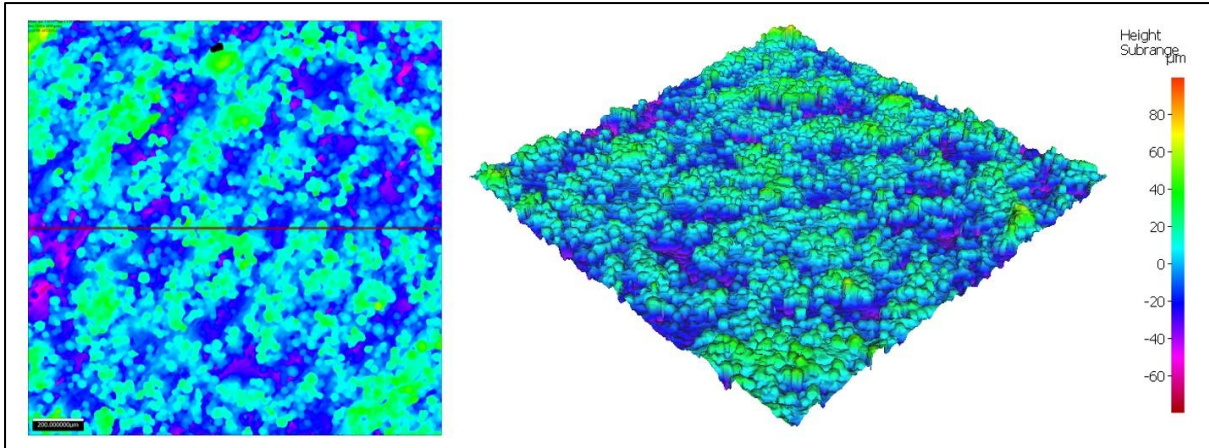


Figure 4.3 2D (left) and 3D (right) views of the surface of a Ti64 sample manufactured by SLM.

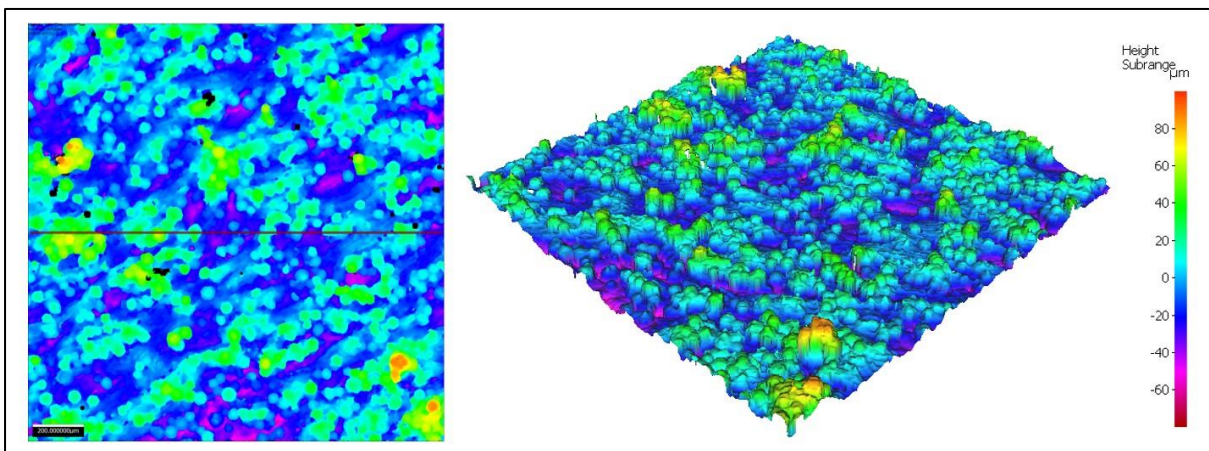


Figure 4.4 2D (left) and 3D (right) views of the surface of a Ti5553 sample manufactured by SLM.

4.1.3 Wettability

Both as-printed Ti64 and Ti5553 proved to have a similar and slightly hydrophilic behaviour, as the water contact angles were $(78.2 \pm 7.2)^\circ$ and $(79.2 \pm 3.6)^\circ$, respectively. These mean values of contact angles were obtained by averaging a set of three measurements per alloy, reported in Table 4.2.

Table 4.2 Contact angle (CA) values measured for as-printed Ti64 and Ti5553 samples.

	CA – Ti64	CA – Ti5553
Measurement 1	86.4°	80.5°
Measurement 2	75.3°	75.0°
Measurement 3	73.0°	81.8°
Mean	78.2°	79.1°
Standard deviation	7.2°	3.6°

4.1.4 Cell imaging

SEM imaging of the samples seeded with Saos-2 cells revealed the presence of a significant number of alive (previous sample preparation) cells on the surface of both materials. Not only were the cells alive, but they also showed an optimal morphology, i.e. flat and stretched, so to better interact with and have higher adhesion on the substrate. As can be noticed in Figure 4.5 for Ti64 and Figure 4.6 for Ti5553, bone-like cells were found to adhere not only in the flatter regions of the 3D-printed samples, but they also seemed to interact with the microspherical features on the surface. In fact, it was repeatedly observed the presence of elongated cells extending from a flatter area to a microparticle nearby, with their filopodia (i.e. finger-like cellular protrusions) anchored on it (Figure 4.5C and Figure 4.6C).

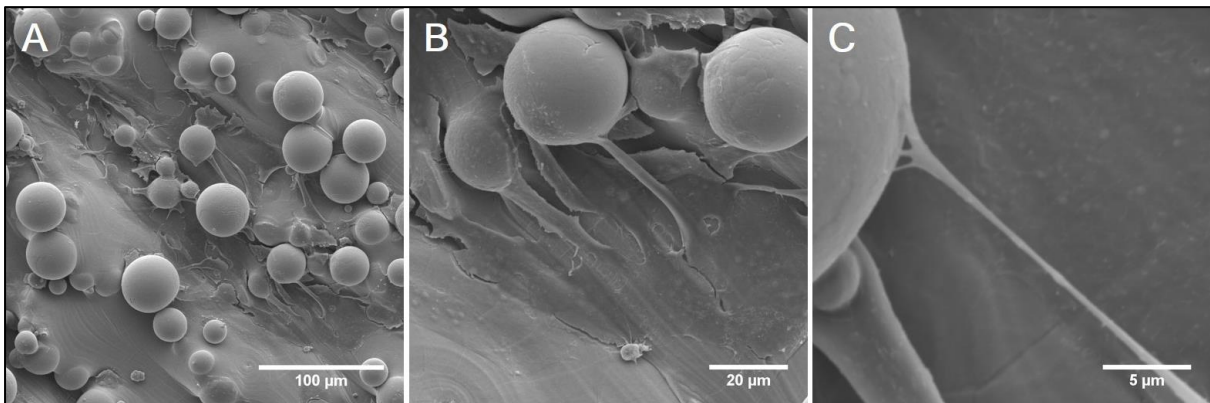


Figure 4.5 SEM micrographs showing bone-like cells adhering on a 3D-printed Ti64 sample. Cells are present both in the flatter areas and stretching from the flatter regions to the microspherical particles. In particular, micrograph C shows a significantly elongated cell anchoring its filopodia onto a microsphere.

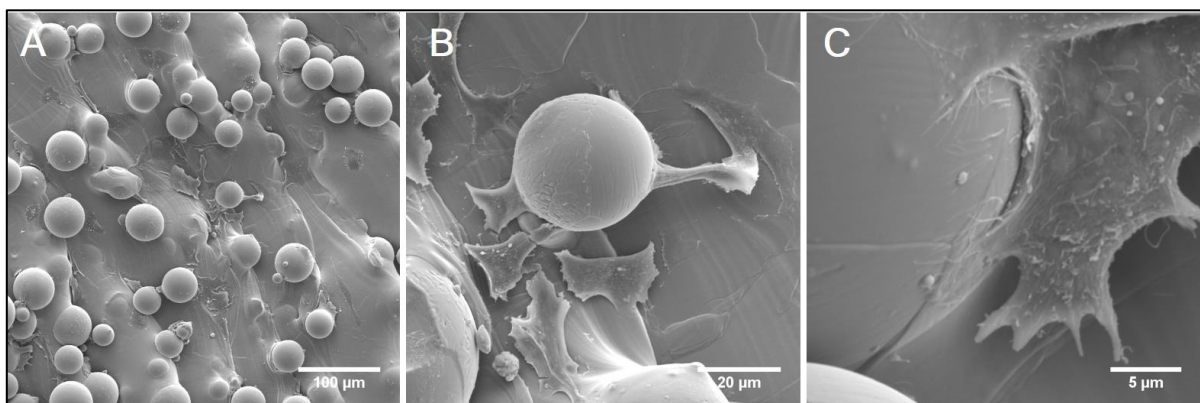


Figure 4.6 SEM micrographs showing bone-like cells adhering on a 3D-printed Ti5553 sample. As in case of Ti64 (Figure 4.5), cells are anchored both to the flatter areas and to the microspherical particles. In particular, a cell adhering on a microparticle is visible in micrograph C.

4.1.5 Bioactivity

Samples of Ti64 and Ti5553 immersed in Hanks' solution for 3 days showed little bioactivity, as very few precipitates were distinguishable on the surface. On the other hand, more precipitates were present after 7-day immersion (Figure 4.7). EDS analysis revealed the presence of elements like P, Ca, Cl and K, which are characteristic of the solution used. Notably, the presence of Ca and P suggested that some precipitates on the surface may have been crystals of hydroxyapatite, and not simply generic salts precipitated from the solution.

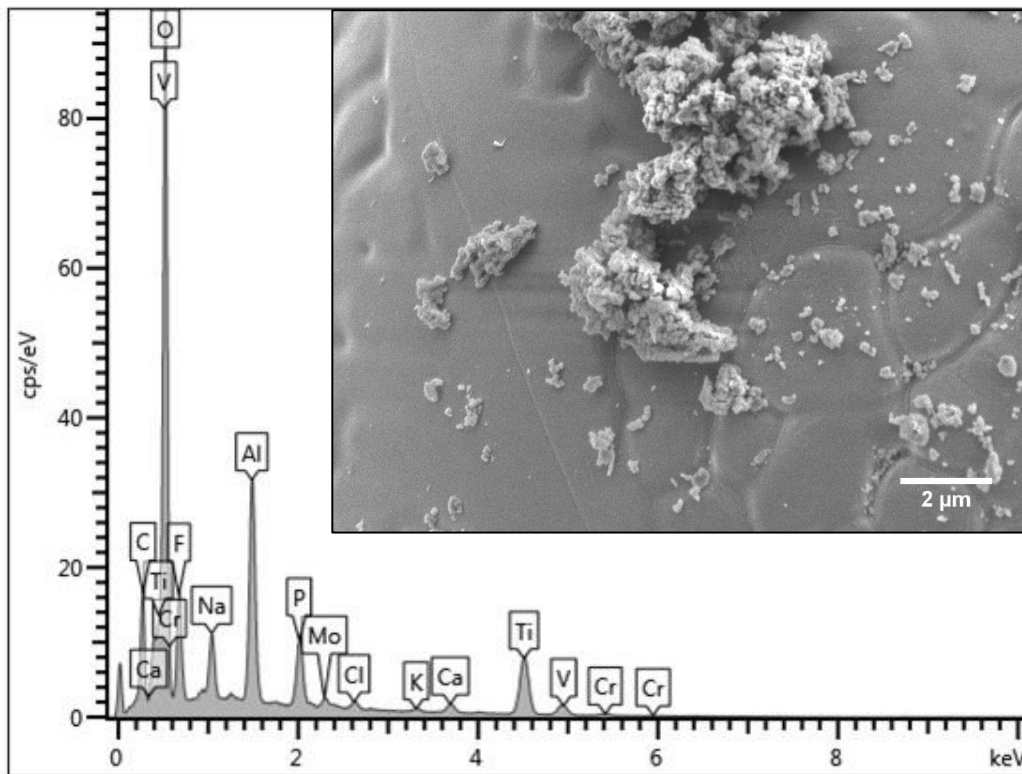


Figure 4.7 SEM image showing some precipitates on the surface of a Ti5553 sample immersed in Hanks' solution for 7 days, and its correspondent EDS analysis. Peaks relative to Ca, K, Cl and P are distinguishable in the EDS spectrum.

4.2 Anodized samples: dual-scale topography

4.2.1 Morphology and topography

In general, anodization of 3D-printed Ti64 and Ti5553 succeeded in the formation of TiO₂ nanotubes. The presence of these nanoscale features together with the microparticles characteristic of the as-printed samples contributed to the creation of a dual-scale surface topography, which was the main goal of this research work.

4.2.1.1 Anodization at constant voltage

Both Ti64 and Ti5553 were anodized at 20 V, 40 V, 60 V and 80 V for 30 minutes following the process described in Section 3.2. In all cases, anodization resulted in the obtainment of arrays of titanium dioxide nanotubes over the entire surface, both on the microparticles and on the underlying substrate. An example of the morphology generated by anodization is given in Figure 4.8.

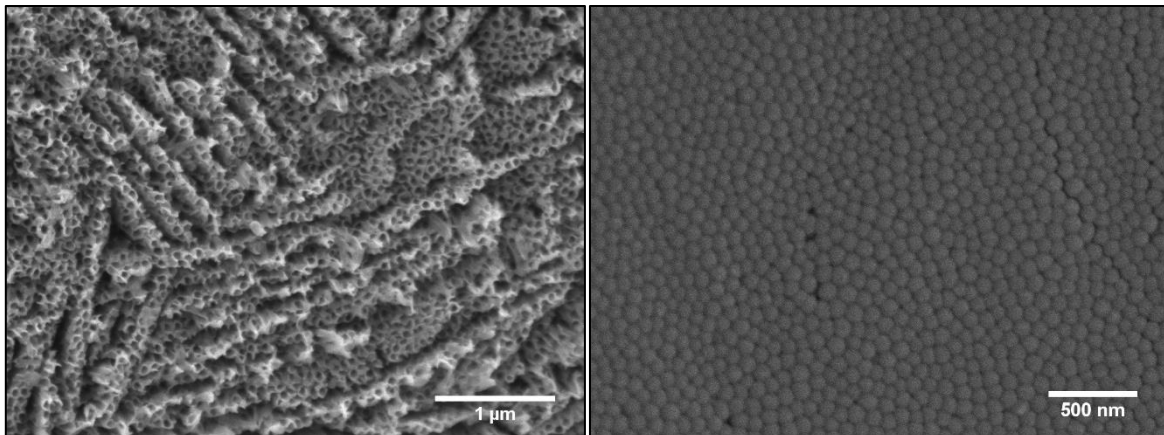


Figure 4.8 Top (left) and bottom (right) views of TNTs. Left and right images correspond to a Ti64 sample anodized for 30 minutes at 60 V and 40 V, respectively.

The process also resulted in the formation of cracks across the surface, especially in the less flat areas and on the microparticles (Figure 4.9). Cracks are due to the outgrowth mechanism of the nanotubes, perpendicularly with respect to the substrate and following its morphology. Therefore, along the curved surfaces they tend to separate into arrays tangent to the regions underneath. Cracks appeared to be more extended for higher anodization voltages, which may be due to the increase in the electrochemical etching. The presence of cracks enabled to have a side-view of the TNTs arrays, as shown in Figure 4.10. This was important to confirm that

anodization did not just form nanopores on the surface, but tubular structures, i.e. TiO₂ nanotubes.

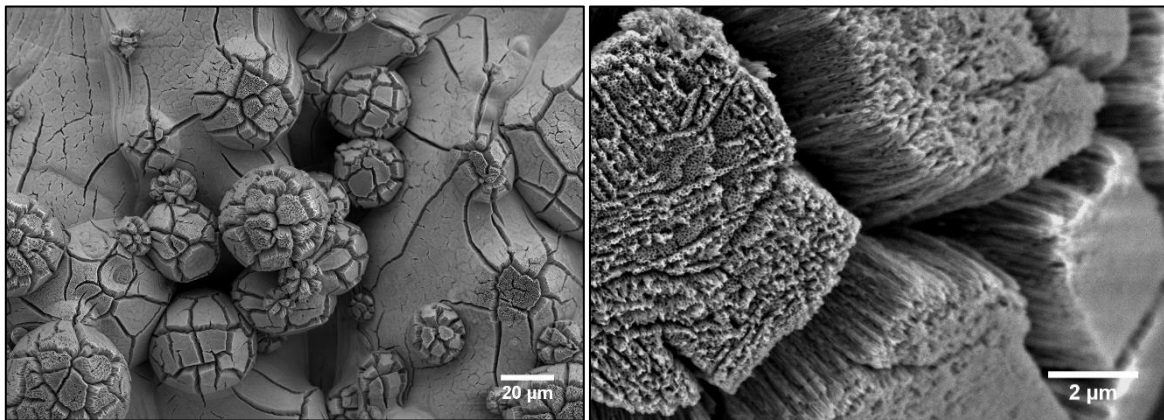


Figure 4.9 Left: Cracks visible on the surface on an anodized Ti64 sample (anodization at 60 V for 30 minutes), in particular across the microspherical particles. Right: Higher magnification image showing TNTs arrays separated by cracks on a microparticle.

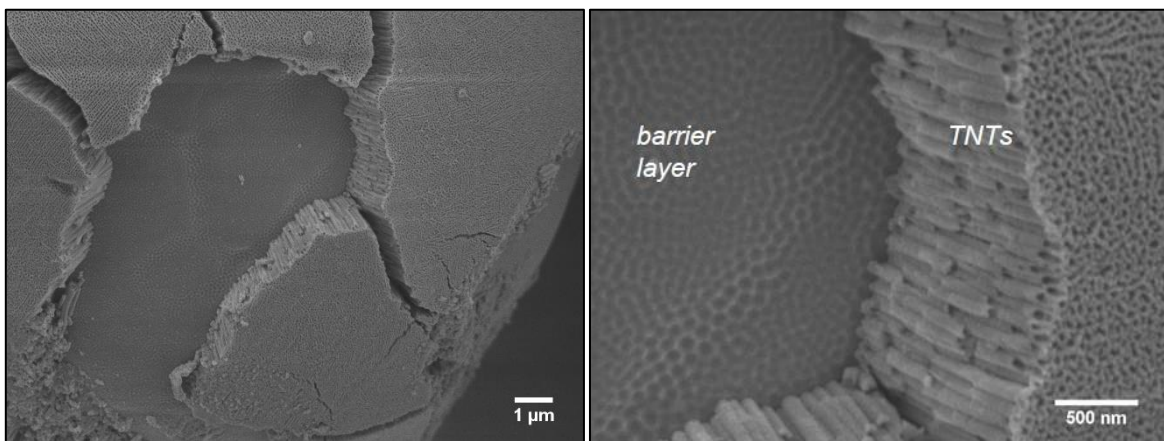


Figure 4.10 Left: Microspherical particle on an anodized Ti64 sample (anodization at 40 V for 30 minutes) with a missing TNTs array, whose detachment may have been promoted by the presence of cracks. Right: Higher magnification image showing a side-view of the TNTs. The barrier layer, i.e. a layer of amorphous TiO₂ that forms in between the substrate and the TNTs [50], is also visible.

Anodization of Ti64 resulted in the creation of well-organized nanotubes arrays on the surface when a voltage of 20 V, 40 V or 60 V was applied. A different behaviour was observed for Ti64 anodized at 80 V. In this case, in several areas there was no evidence of tubular structures although some nanotubes were still identified on the surface. The reason is that electrochemical etching increases at higher voltages, and this in turn makes the tube wall thinner, especially at the top where etching is more intense. Therefore, TNTs generated at 80 V started to disintegrate and collapse onto the neighbouring tubes, merging into each other and leading to the formation of a disordered TiO₂ structure, shown in Figure 4.11. This structure is usually referred to as “nanograss”, and it constitutes a quite common and undesired outcome of anodization

processes [55]. Nanograss was often noticed also on samples anodized at lower voltages (20, 40 and 60 V), but less extended than that formed at 80 V.

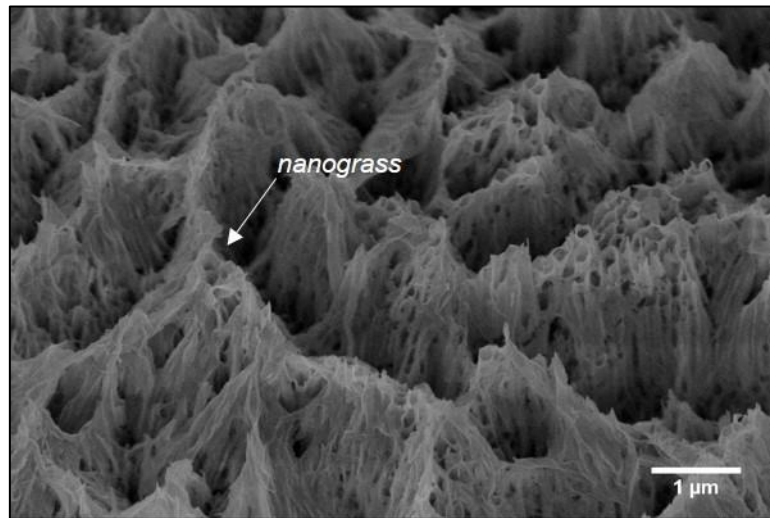


Figure 4.11 SEM image of a Ti64 sample anodized at 80 V for 30 minutes, in which it is visible how several TNTs collapsed and merged into each other forming nanograss.

Arrays of TiO_2 nanotubes were obtained on the surface of Ti5553 for all the four different anodization voltages investigated. In contrast to what observed for Ti64, nanotubes were consistently created also at a voltage equal to 80 V, even though significantly extended formations of nanograss were identified in some areas of the surface. In general, nanotube architecture seemed to be less stable in the case of Ti5553 than Ti64, as the TNTs often appeared less intact and cracked at the top, leading sometimes to the formation of vast regions of nanograss. Moreover, some inconsistencies in the TNTs morphology were noticed for Ti5553 samples, such as nanotubes that seemed to have a double wall (Figure 4.12).

Differences in the behaviour of Ti64 and Ti5553 when anodized can be attributed to the different quantity and type of alloying elements. In fact, different elements can show different electrochemical oxidation rates, thus different reaction rates leading to selective dissolution [18]. This may also constitute the reason why some anomalies were detected for anodized Ti5553 samples.

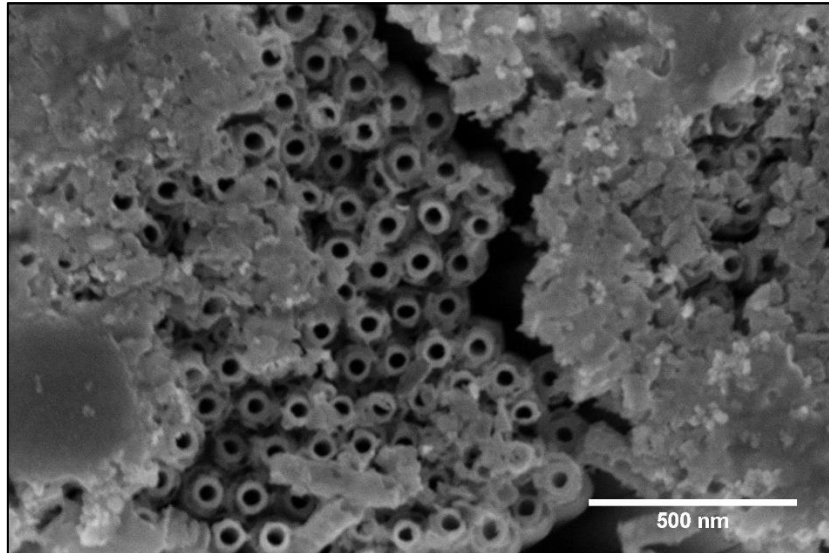


Figure 4.12 Example of anomalous TNTs obtained by anodizing Ti5553 at 60 V for 30 minutes. Nanotubes seems to have a double wall, and extended regions of nanograss are present.

4.2.1.2 Influence of voltage on TNTs diameter

To evaluate the influence of the anodization voltage on the nanotubes diameter, Ti64 and Ti5553 were anodized for the same length of time (30 minutes) using four different voltages, namely 20 V, 40 V, 60 V and 80 V. SEM images representative of the TNTs obtained at each condition are shown in Figure 4.13 for Ti64 and in Figure 4.14 for Ti5553. For every case, TNTs diameter was measured following the methodology illustrated in Section 3.3.1.1. For what concerns Ti64 anodized at 80 V, it was possible to analyze a SEM image corresponding to a microparticle only, as TNTs with a morphology suitable for detailed measurements were not identified in the flatter regions of the sample. In regard to Ti5553, areas showing the anomalies mentioned before (Section 4.2.1.1) were excluded from the analysis, and only regions with TNTs with a consistent morphology were taken into account. The results obtained for both the alloys at each anodization voltage are reported in Table 4.3.

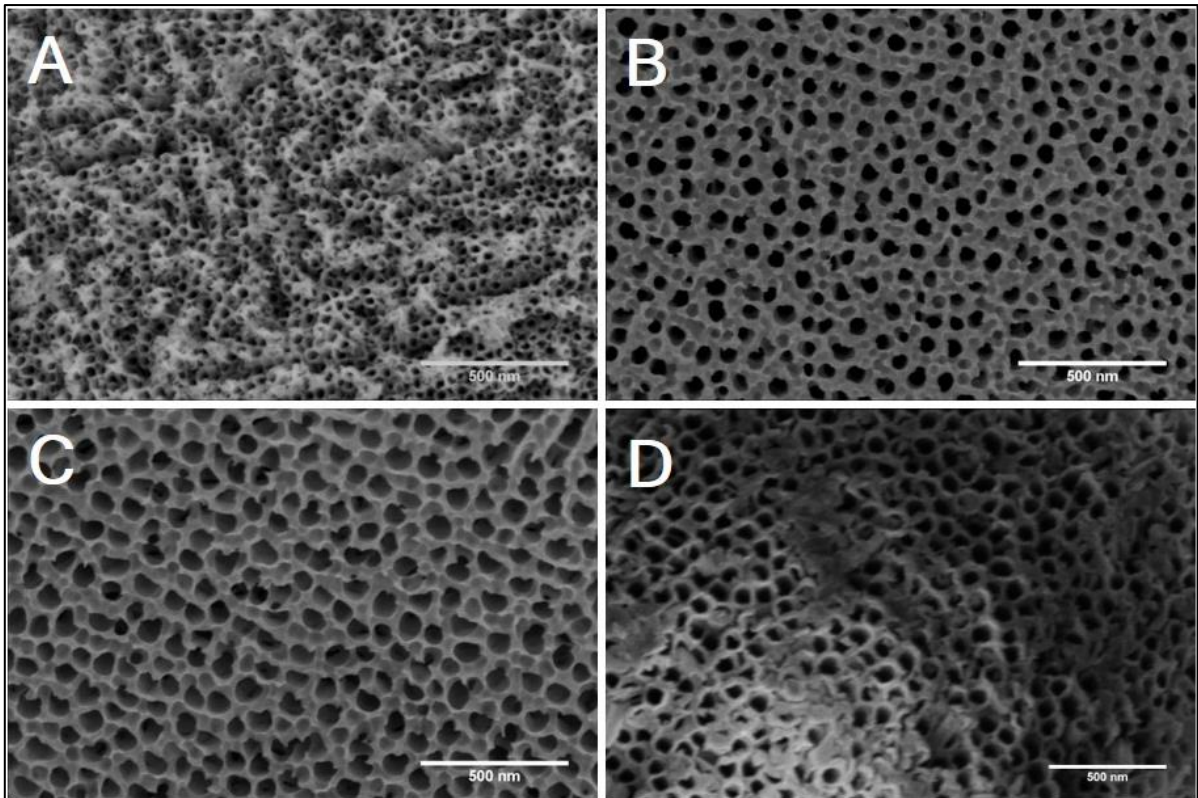


Figure 4.13 SEM images of TNTs generated by anodization of Ti64 for 30 minutes at 20 V (A), 40 V (B), 60 V (C) and 80 V (D).

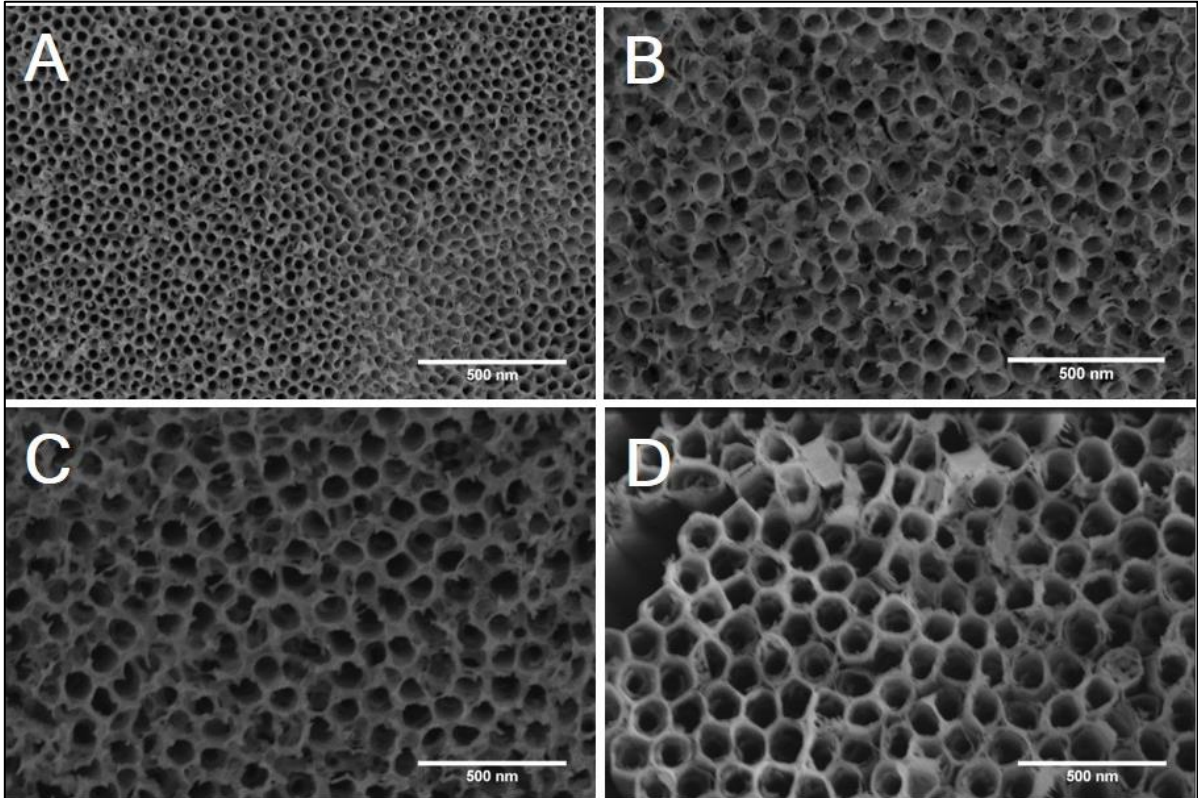


Figure 4.14 SEM images of TNTs generated by anodization of Ti5553 for 30 minutes at 20 V (A), 40 V (B), 60 V (C) and 80 V (D).

Table 4.3 Mean diameter of TNTs generated by anodization of Ti64 and Ti5553 for 30 minutes at four different voltages.

Voltage [V]	TNTs diameter for Ti64 [nm]	TNTs diameter for Ti5553 [nm]
20	22.1 ± 5.6	26.5 ± 6.4
40	47.3 ± 8.9	52.2 ± 9.8
60	67.5 ± 10.6	87.2 ± 8.8
80	59.1 ± 5.2	97.0 ± 15.4

With the exception of Ti64 anodized at 80 V, it was observed that the nanotube diameter increased with the applied voltage. For both the alloys, the differences in the values obtained at each voltage were statistically significant, as verified by Student's *t*-test. As can be observed from the values in Table 4.3, TNTs of Ti64 anodized at 80 V showed a diameter lower than those of Ti64 anodized at 60 V, in contrast to what was expected. It is believed that Ti64 anodized at 80 V differ from the common trend due to extensive electrochemical etching which caused the collapsing of the nanotubes into nanograss. TNTs with larger diameters might have proved to be more unstable, thus etching may have been more substantial for them leading to their disintegration. This in turn could explain why only smaller TNTs preserved their tubular architecture, and thus only areas with smaller nanotubes were identifiable to be used for further analysis.

The TNTs diameter was observed not only to increase with the applied voltage, but to do so following a linear trend. This was valid for both the alloys at every condition tested, excluding the case of Ti64 anodized at 80 V, as already discussed. The graph in Figure 4.15 reports the variation of the TNTs diameter (data used were those reported in Table 4.3) as a function of the applied voltage. The data points fit a linear regression model well, enabling to identify a trendline with a high coefficient of determination (R^2 tending towards 1). The slope of the trendline was computed to be equal to 1.14 and 1.30 for Ti64 and Ti5553, respectively. Ti64 anodized at 80 V was omitted from this analysis, as it did not follow the expected linear trend.

Finally, it was observed that TNTs on Ti5553 showed a larger diameter than those on Ti64 at every anodization voltage, and Student's *t*-test proved the difference to be statistically significant in all cases.

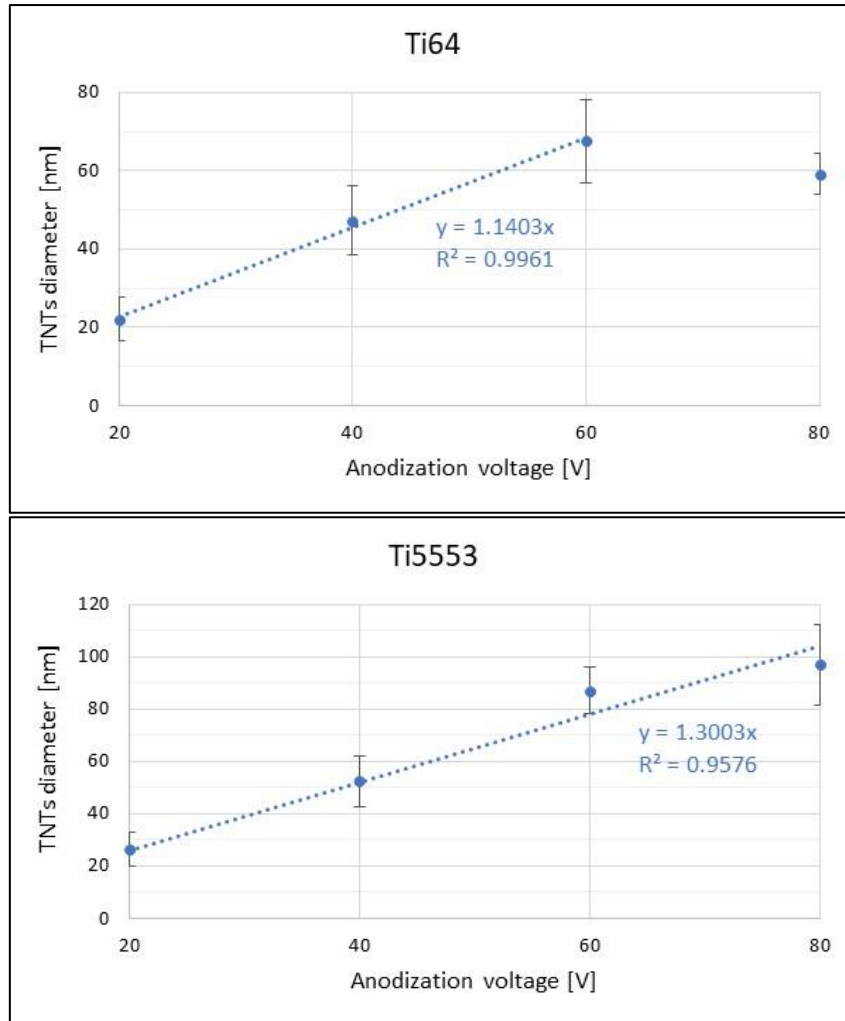


Figure 4.15 Graphs showing the variation in TNTs diameter as a function of the anodization voltage for both Ti64 and Ti5553.

4.2.1.3 Influence of time on TNTs morphology

Ti64 and Ti5553 were anodized at a constant voltage of 40 V for four different lengths of time, i.e. 5, 10, 20 and 60 minutes, to evaluate the influence of time on TNTs formation and morphology.

Figure 4.16 and Figure 4.17 show how the nanotubes morphology evolved over time for Ti64 and Ti5553, respectively. In both cases it was noticed that after 5 minutes the surface was mainly characterized by the presence of nanopores rather than nanotubes. Some tubular structures were identified, but there was no evidence of significantly extended arrays of TNTs. Samples anodized for 10 minutes showed a similar behaviour, but pores were higher in number and seemed to start assuming an ordered pattern. After 20 minutes, well-organized arrays of TNTs were present on the entire surface of both Ti64 and Ti5553, with a morphology close to

that observed for an anodization time of 30 minutes, explained in more detail before (Section 4.2.1.1). TNTs were still noticeable after 60-minute long anodization, but in some areas extended nanograin structures were observed, in agreement with the fact that nanograin is usually more widespread for longer anodization time.

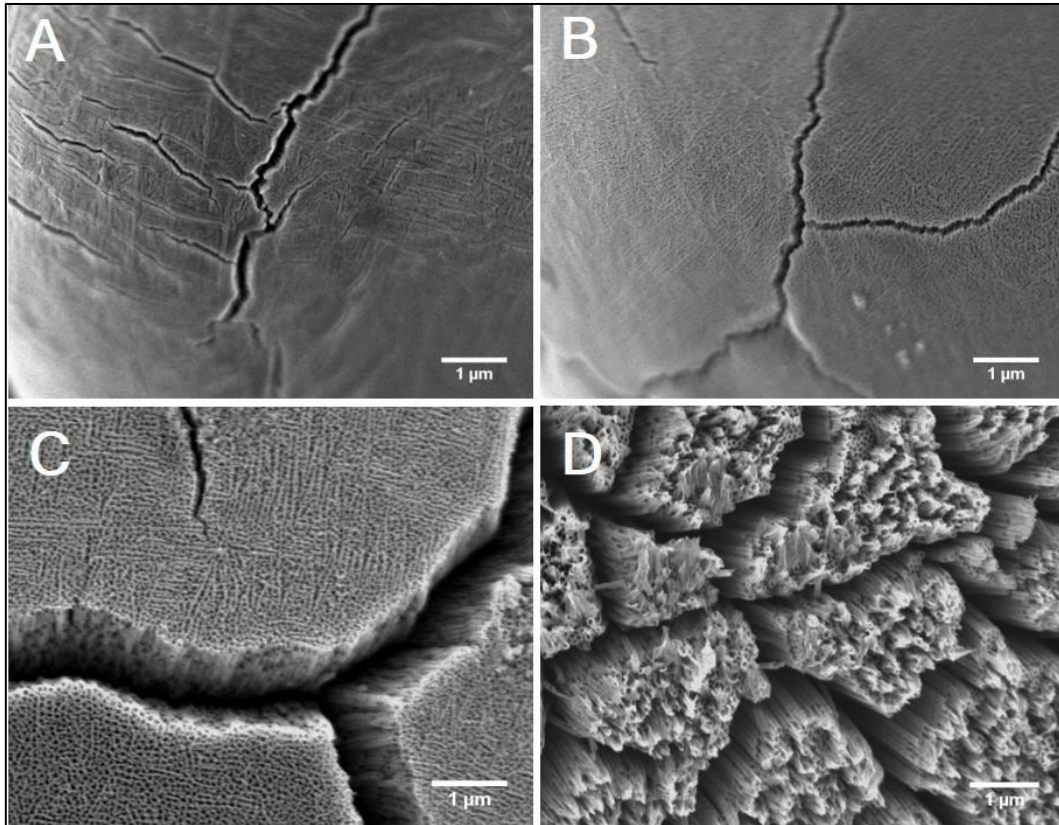


Figure 4.16 Morphology of TNTs on Ti64 anodized at 40 V for 5 (A), 10 (B), 20 (C) and 60 (D) minutes.

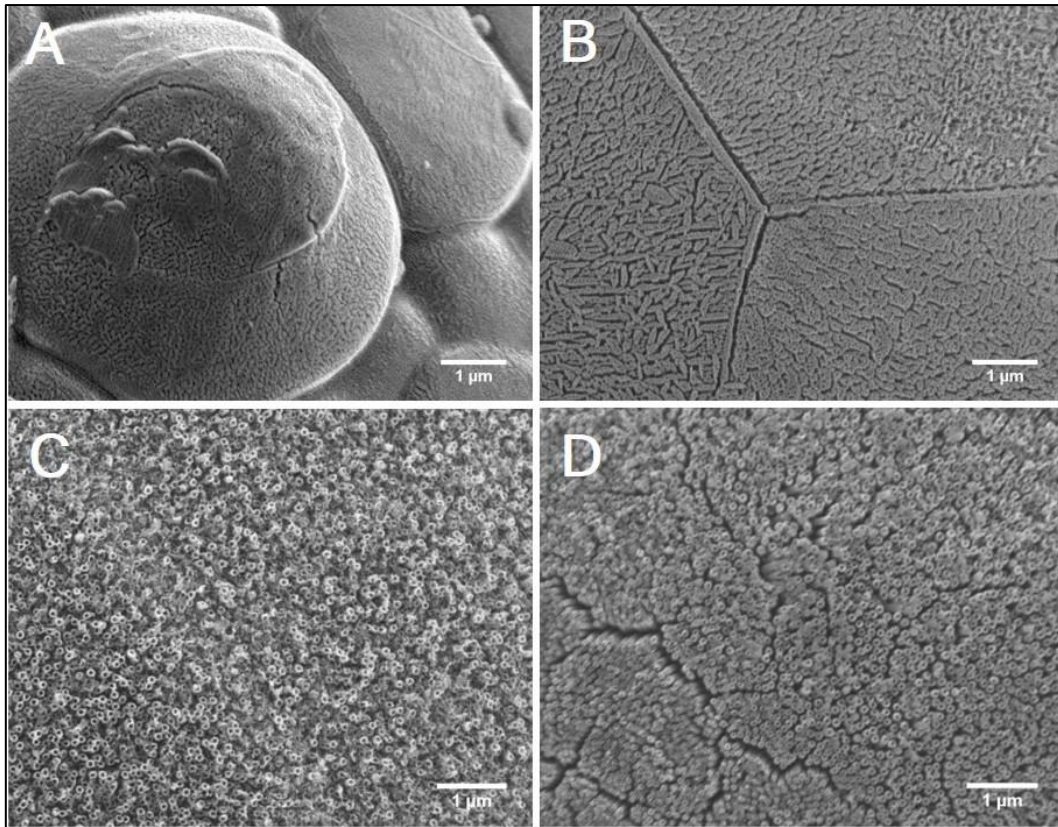


Figure 4.17 Morphology of TNTs on Ti5553 anodized at 40 V for 5 (A), 10 (B), 20 (C) and 60 (D) minutes.

4.2.1.4 Anodization with initial stepwise increase of voltage

Ti64 and Ti5553 were anodized with an initial stepwise increase of voltage of 1 V every 10 seconds, until a voltage of 40 V was reached and then maintained constant for 30 minutes (Figure 3.2). The objective was to assess eventual differences in the outcome of the process and in the TNTs morphology if compared to Ti64 and Ti5553 anodized at a constant voltage of 40 V (instantly applied at the start and kept constant for the entire process). For the sake of simplicity, anodization at constant voltage will be indicated as case I, while anodization with initial stepwise increase of voltage will be referred to as case II.

Well-ordered arrays of TNTs were successfully created both for Ti64 and Ti5553 under case II process conditions (Figure 4.18). Moreover, the nanotubes were found to be distributed over the entire surface of the samples, as obtained for case I as well (Section 4.2.1.1). Case II TNTs morphology did not appear to be different to that of case I. Features such as nanograss and cracks, commented in Section 4.2.1.1 for case I, were identified in case II as well. The lack of visible differences between case I and case II led to the conclusion that the initial stepwise increase of voltage did not affect the outcome of the process in terms of surface characteristics and TNTs morphology. This result may be strictly linked to the specific stepwise increase used,

and different outcomes may be obtained using other conditions, such as increasing the voltage at a different speed or with a linear trend, or reducing the anodization time.

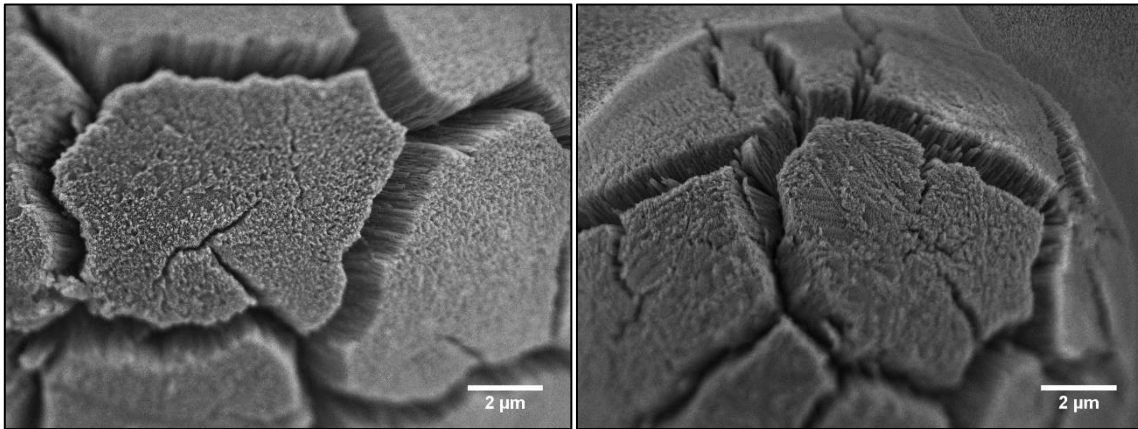


Figure 4.18 TNTs obtained on Ti64 (left) and Ti5553 (right) by applying an initial stepwise increase of voltage.

4.2.2 Wettability

Both Ti64 and Ti5553 anodized at a constant voltage of 20 V, 40 V, 60 V and 80 V for 30 minutes proved to be highly hydrophilic, as in all cases significant spreading of water on the surface occurred. It is reasonable to assume that water not only spread onto the surface, but also inside the nanotubes.

Water contact angles measured for both alloys at the different anodization conditions were all below 15° (Table 4.4), much lower than those of the as-printed samples (Section 4.1.3). Therefore, it can be concluded that anodization led to a substantial increase in hydrophilicity for both the materials under investigation. An example of the different wetting behaviour of the as-printed samples compared to those anodized is shown in Figure 4.19, where the dissimilar interaction of a water droplet with the two surfaces can be observed.

Table 4.4 Mean values of water contact angles (CA) obtained for both Ti64 and Ti5553 at four different anodization voltages (20, 40, 60 and 80 V).

Anodization voltage	CA – Ti64	CA – Ti5553
20 V	(13.0 ± 1.1)°	(9.7 ± 3.4)°
40 V	(11.6 ± 2.3)°	(9.6 ± 1.1)°
60 V	(12.6 ± 1.4)°	(13.3 ± 4.9)°
80 V	(9.8 ± 0.8)°	(9.8 ± 1.5)°

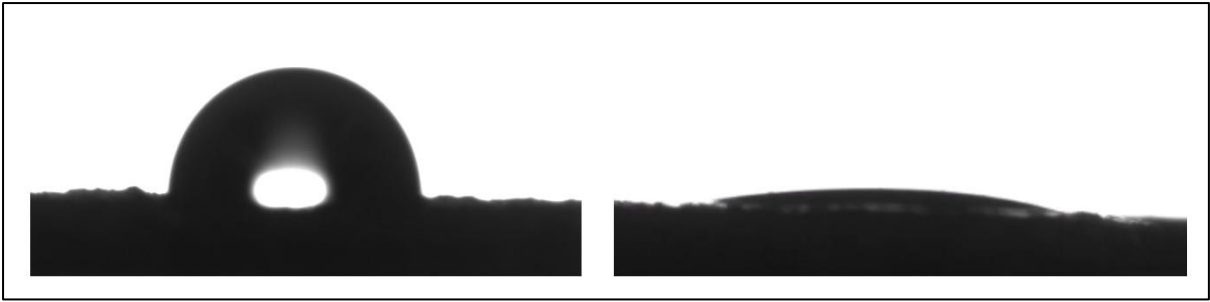


Figure 4.19 Water droplet behaviour on as-printed Ti64 (left) and after anodization at 40 V for 30 minutes (right). The anodized sample showed higher hydrophilicity, as can be inferred by the significant spreading of water (right). A similar behaviour was observed for different anodization voltages and for Ti5553 as well.

4.2.3 Annealing

As shown in Figure 4.20, SEM imaging proved that annealing did not induce any evident change in the morphology of the TNTs arrays, and the nanotube architecture was preserved for both Ti64 and Ti5553. Moreover, XRD analysis proved that annealing induced a phase transformation of the amorphous titania layer, as presence of anatase was detected (Figure 4.21 and Figure 4.22).

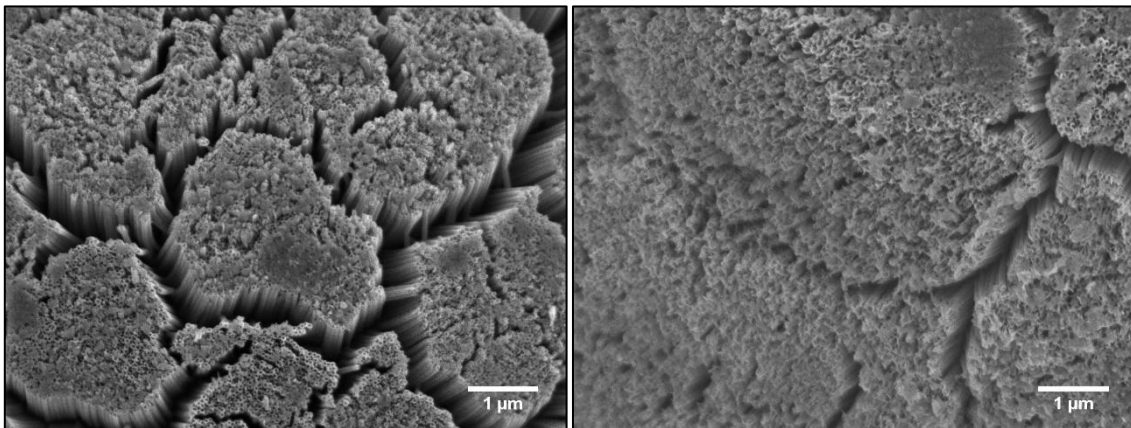


Figure 4.20 TNTs on Ti64 (left) and Ti5553 (right) anodized at 40 V for 30 minutes and then annealed in open air at 500 °C for 2 hours.

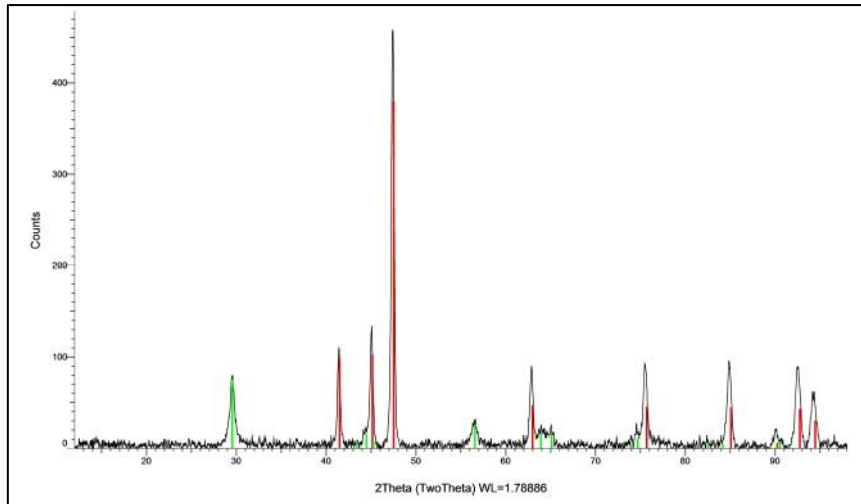


Figure 4.21 XRD spectrum of an anodized and annealed Ti64 sample. Peaks identified by green lines correspond to anatase. Red lines indicate titanium, most likely from the substrate underneath the TNTs film.

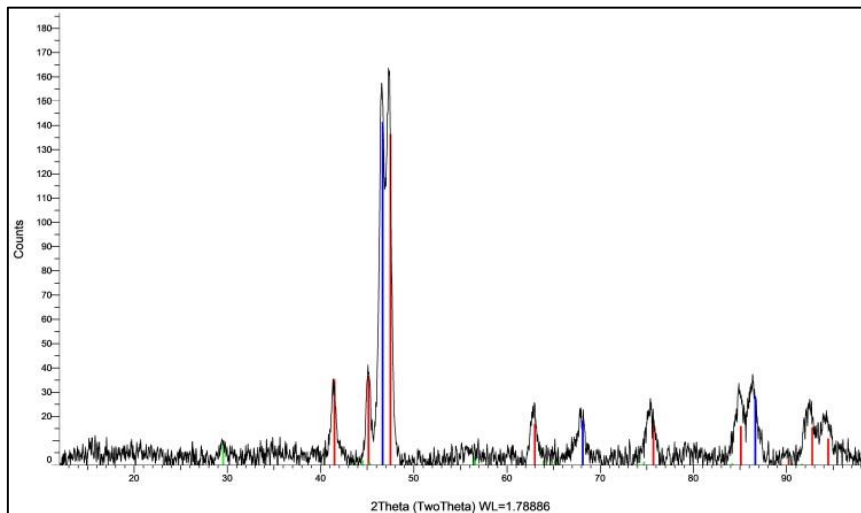


Figure 4.22 XRD spectrum of an anodized and annealed Ti5553 sample. Peaks identified by green lines correspond to anatase. Red lines indicate titanium, most likely from the substrate underneath the TNTs film. A compound of titanium-vanadium-chromium (0.7Ti-0.1V-0.2Cr) was also detected (peaks marked by blue lines).

4.2.4 Cell imaging

Samples of Ti64 and Ti5553 anodized at 40 V for 30 minutes were seeded with Saos-2 cells and prepared for SEM imaging as described in Section 3.3.2.1. Cells were identified on the surface of both substrates. Overall, cells were characterized by a flat morphology and seemed to be well-adhering on the surface and to interact with the TNTs on it, as their filopodia appeared to grow into the nanotubes (Figure 4.23). Analogously to what observed for the as-printed samples (Section 4.1.4), cells were present both in the flatter regions and stretching from these areas to the microspheres nearby (Figure 4.24). In addition, cells seemed to interact with the microparticles on the surface more than what observed for the as-printed samples. The

different behaviour can be attributed to the presence of TNTs, which promoted the adhesion of cells also on the microparticles, that otherwise may not show suitable features to facilitate cell-surface interactions.

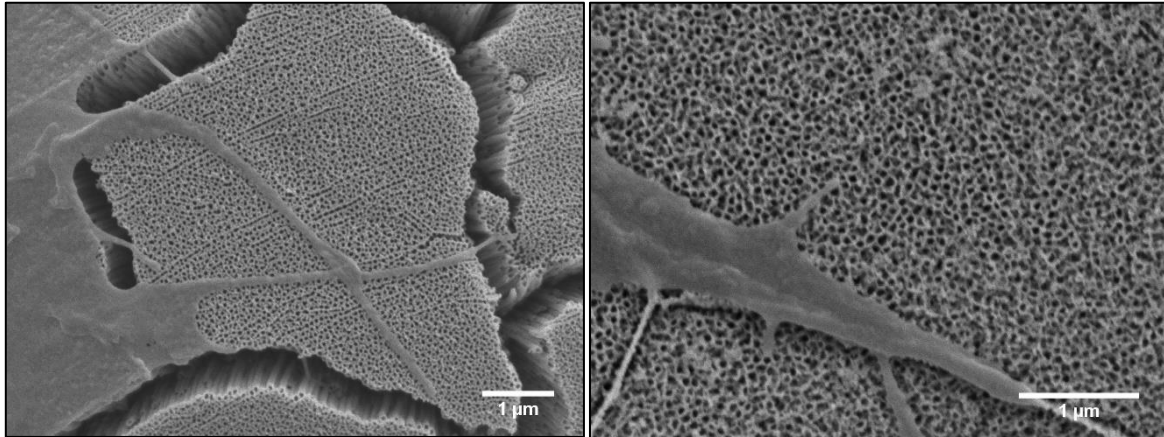


Figure 4.23 SEM micrograph showing cell filopodia interacting with TNTs on the surface of anodized Ti64 (left) and Ti5553 (right) samples.

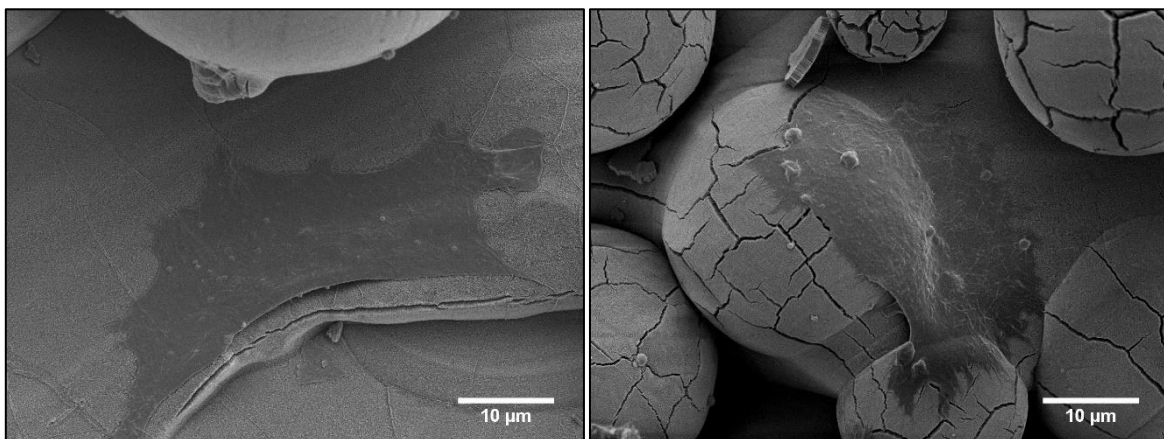


Figure 4.24 Left: Cell on a flat area of an anodized Ti5553 sample. Right: Cell adhering both on some microparticles and on a flat region of an anodized Ti64 sample.

4.2.5 Bioactivity

Some precipitates were observed on the surface of both as-anodized and anodized and annealed samples of Ti64 and Ti5553 after immersion in Hanks' solution for 3 and 7 days. EDS analysis identified elements such as P, Ca, Na, Mg and K, which are all contained in the Hanks' solution used. In particular, the presence of P and Ca may be indicative of hydroxyapatite. It is hence believed that precipitation of some salts from the solution and nucleation of hydroxyapatite crystals occurred although difficult to be clearly detected by SEM imaging. Therefore, it was hypothesized that salts and HA mostly precipitated inside the nanotubes, filling their cavities and growing on the top of them. For example, TNTs in Figure 4.25 appeared to be closed on

the top, probably due to the precipitates filling them up to the top and thus turning into a coating.

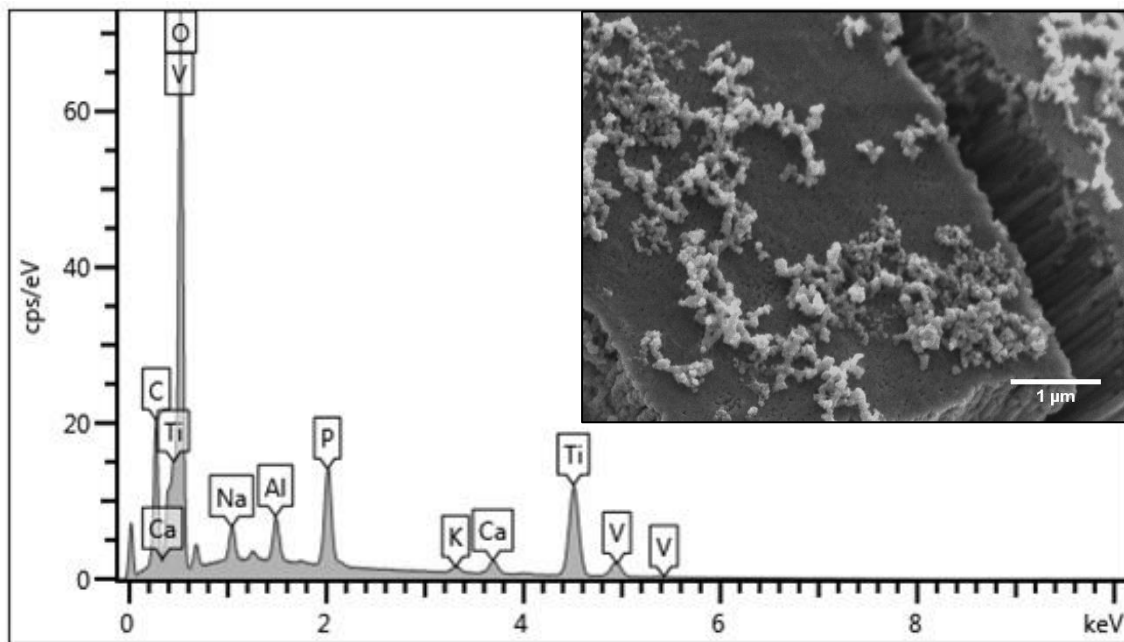


Figure 4.25 EDS spectrum and SEM image of an anodized Ti64 sample immersed in Hanks' solution for 3 days. Precipitates of Ca, P, Na and K and P are visible, and it seems that they filled the TNTs, as nanotubes pores are no longer noticeable on the surface.

5. Discussion

Bone implants with a microscale surface topography have been shown to have an improved ability to osseointegrate [3]. Selective laser melting has emerged as a promising technique to manufacture implants mainly due to the possibility to manufacture highly customized parts, to better meet patient-specific needs, and inherently microrough components [24]. Previous work has already demonstrated the use of SLM for the fabrication of microrough parts of both Ti64 [25] and Ti5553 [56]. A typical feature of substrates manufactured by SLM is their surface covered by randomly distributed microspherical particles, mainly traces of unmelted feedstock powders [26]. Ti64 and Ti5553 samples used in this work showed this characteristic morphology (Figure 4.1), concordantly to what reported in other studies [25], [28]. While the manufacturing of Ti64 using SLM has already been investigated for biomedical applications [28], [29], to our knowledge studies on the use Ti5553 in this field have not been reported. However, being Ti5553 a metastable β alloy, it could be a suitable candidate as a bone implant material, due to its lower elastic modulus, closer to that of bone [7].

Not only microscale, but also nanoscale surface topography is believed to play a key role in promoting bone cell functions, and thus osseointegration [31]. To this regard, anodization of titanium to create TiO₂ nanotubes has been intensively investigated [48], [49], [52]. Several studies reported an improvement in cell adhesion, proliferation and differentiation determined by the presence of these nanostructured features [50], [57]. Electrochemical anodization is a promising surface modification technique because, thanks to their self-ordering nature, well-ordered arrays of TNTs can be obtained even on substrates with complex geometries, which is fitting for bone implants. Moreover, electrochemical anodization permits high control over the nanotube size by properly selecting process parameters like electrolyte composition, time and voltage [44]. As cell-surface interactions are highly influenced by topographical clues, the possibility to easily produce surface features with highly-specific dimensions makes it possible to better control such interactions, and, ultimately, osseointegration [31]. Studies have shown how bone cell responses are influenced by TNTs diameter [58], which is mainly dependent on the anodization voltage [44]. Therefore, it was considered of importance for this research to analyze in detail on how the nanotube size was controlled by the applied voltage for both Ti64 and Ti5553 produced by SLM. For both materials, a linear relationship between the two variables was identified. This is in agreement to what previously observed for flat titanium

substrates [44], [52], thus neither the use of different Ti-based materials nor the use of samples with a microscale topography altered the expected trend.

Given the advantages of both micro- and nanoscale on enhancing osseointegration, Maher et al. [29] and Gulati et al. [28] proposed a new generation of Ti implants that combines these two scales. They created this unique dual topography by electrochemically anodizing Ti64 samples manufactured by SLM, so that nanoscale of TNTs and microscale characteristic of SLM can be combined. A similar approach was applied in this work with two Ti alloys, i.e. Ti64 and Ti5553. Although the present study adopted some different conditions both in the SLM manufacturing (layer thickness, sample geometry, materials) and in the anodization stages (electrolyte composition, counter-electrode, process parameters), the results obtained were analogous to those presented in [28] and [29]. In particular, this work proved the electrochemical anodization of SLM substrates to be successful not only for Ti64, but also for Ti5553. To our knowledge, anodization of Ti5553 manufactured by SLM has never been reported.

In agreement with observations by Gulati et al., anodization of curved surfaces led to the formation of cracks in the TNTs film, as a consequence of the growth mechanism of nanotubes and internal stresses [59]. The presence of cracks may compromise the stability of the TNTs and their adhesion to the substrate. Concerning this, detachment of the anodic coating was sometimes observed in localized areas of the samples under investigation, as shown in Figure 4.10. Poor bonding of the TNTs film to the surface of a bone implant can be detrimental for the success of implant itself, therefore anodization of complex geometries, which are typical of bone implants, without cracks is desirable [59]. In this work, we attempted to reduce crack formation by using a slow voltage ramping approach, unfortunately with no significant effect on crack reduction. Coating adhesion was also not possible to measure through standard procedures such as scratch testing, due to the inherent microroughness of the SLM substrate.

Anodized Ti64 and Ti5553 samples showed higher hydrophilicity compared to as-printed substrates, as TiO₂ nanotubes typically show a hydrophilic behaviour, as proved by others as well [60]. The increase in hydrophilicity could be beneficial in the context of bone implants, as hydrophilic surfaces can promote the initial interactions between the surface itself and the wetting liquid, which is an important aspect for both wound healing and osseointegration [61].

SEM imaging after Saos-2 culturing showed that the cells well adhered on the surface of both as-printed and as-anodized Ti64 and Ti5553 samples. In particular, it was observed that cells greatly interacted with the nanotubes, as their filopodia were noticed to be extended inside the nanotubes themselves. An analogous behaviour was reported by others as well [62]. Some studies present in literature further corroborated the hypothesis that TNTs can influence and improve cell responses with *in vitro* tests [57]. Moreover, improvement in osteoblast adhesion was found for substrates with a dual-scale topography [28], [29]. Future work will probe the time-resolved response of cells to these substrates.

It is believed that further enhancement in cell responses can be achieved by annealing after anodization. In fact, annealing can promote the phase transformation of the amorphous as-anodized TiO₂ layer into the crystalline forms of rutile and/or anatase, which are considered to improve cell adhesion [62]. Selection of suitable annealing parameters, especially time and temperature, is important, as the phase transformation induced by annealing can cause the collapse and disintegration of the TiO₂ nanotubes, with consequent loss of nanotubular architecture [63]. Annealing conditions used for this research were identified based on previous studies [62] not to have this undesired outcome, which was, in fact, avoided. XRD analysis on the annealed Ti64 and Ti5553 samples detected the presence of anatase, in agreement with other studies [62], [63].

Finally, surface modification to generate TNTs can be beneficial for improving bioactivity, which can be poor in case of machined Ti-based bone implants. Higher bioactivity is important to promote the bonding between implant and host tissue, i.e. to increase osseointegration [1]. *In vivo* bioactivity of a material can be predicted by evaluating its apatite-forming ability, which can be assessed in a simulated body fluid [64]. Preliminary investigations carried out in this work identified the presence of precipitates of Ca and P, indicative of apatite, on the surface of Ti64 and Ti5553, especially when TNTs are present. This seems to confirm the improvement in bioactivity related to TNTs proved in other studies [65].

6. Conclusions

6.1 Summary of major findings

The present research reached its main objective of creating TiO₂ nanotubes by electrochemical anodization of Ti64 and Ti5553 samples manufactured by SLM. In particular, to our knowledge, anodization of 3D-printed Ti5553 samples has not been previously investigated. For both the alloys used, a dual-scale surface topography was obtained by combining microscale of 3D-printed substrates and nanoscale of TNTs generated by anodization. Implants with such dual-scale topography have been proposed as the new generation of multi-functional bone implants, able to improve osseointegration while addressing at the same time other issues such as drug delivery [28].

Study on the influence of voltage on the nanotubes diameter proved anodization to be an easy way to control the size of the nanoscale features generated by adjusting process parameters. Previous work already outlined the linear dependence of diameter on voltage in case of TNTs on flat titanium substrates [44], [52], and this research confirmed this trend to be valid also in case of two different titanium alloys, i.e. Ti64 and Ti5553, and for samples with an initial microscale surface topography.

Anodization of 3D-printed samples contributed not only to the creation of a dual-scale surface topography, but also led to a significant increase in surface hydrophilicity, which could be beneficial for osseointegration and wound healing.

Annealing after anodization did not cause alteration in the nanotubular architecture and succeeded in the transformation of amorphous TiO₂ into anatase, which can improve cell adhesion [62].

Cell imaging by SEM showed that the substrates, both as-printed and as-anodized, were not cytotoxic, and showed bone-like cells to be well-adhered on the surface. In particular, promising interaction between cell filopodia and nanoscale surface features, namely TNTs, was observed for the anodized samples. The two alloys share similar morphology, while having different composition, and no apparent difference in cellular response was noted. Further cellular assays over longer periods of time would be needed to determine if the alloy composition affects cellular activity.

Finally, presence of Ca and P precipitates on the surface of the samples immersed in SBF Hanks' solution is considered promising for what concerns their bioactive properties.

6.2 Limitations and future directions

Although anodization succeeded in the creation of well-ordered arrays of TNTs, the process also resulted in generation of cracks on the curved substrates employed. This could constitute a potential limitation to its employability with bone implants, as they often have complex geometries. Further tests should be done to assess whether the presence of cracks may compromise the stability and adhesion of the TNTs film to the substrate underneath.

Cell imaging provided some qualitative preliminary information about the interaction of bone-like cells and the substrates under investigation. However, more detailed studies on their biocompatibility would be fitting, as such substrates are representative of possible material systems for manufacturing bone implants. Therefore, further investigations would involve *in vitro* tests to quantitatively assess cellular responses by determining, for example, cell metabolism, which in turn can provide information on cell viability, and ability to promote new bone growth. *In vitro* studies would be also useful to better compare and highlight eventual dissimilarities in the two alloys employed in this research (Ti64 and Ti5553) and in the three different groups of samples investigated (as-printed, as-anodized, and anodized and annealed).

In vitro tests could provide indicative information about cell responses to the substrates under analysis, but they still would not be sufficient to assess osseointegration. In fact, when collocating this project in the broader scenario of bone implants, its ultimate goal is to determine whether or not dual-scale topography can improve osseointegration. Therefore, it would be necessary to do some *in vivo* studies to really investigate the ability to osseointegrate of the as-printed, as-anodized, and anodized and annealed samples, for both Ti64 and Ti5553.

Finally, TNTs could be loaded with a therapeutic agent to realize drug-eluting TNTs-Ti implants. Furthermore, coating of the drug-loaded nanotubes with a biodegradable polymer could be also investigated to better control the drug release kinetics by adjusting the polymer degradation rate [66].

References

- [1] D. A. Puleo and A. Nanci, "Understanding and controlling the bone implant-interface," *Biomaterials*, vol. 20, no. 23–24, pp. 2311–21, 1999.
- [2] N. R. Van, "Titanium: the implant material of today," *J. Mater. Sci.*, vol. 22, pp. 3801–3811, 1987.
- [3] S. Bauer, P. Schmuki, K. von der Mark, and J. Park, "Engineering biocompatible implant surfaces: Part I: Materials and surfaces," *Prog. Mater. Sci.*, vol. 58, no. 3, pp. 261–326, 2013.
- [4] K. Grandfield, "Bone, implants, and their interfaces," *Phys. Today*, vol. 68, no. 4, pp. 40–45, 2015.
- [5] S. Kurtz, K. Ong, E. Lau, F. Mowat, and M. Halpern, "Projections of primary and revision hip and knee arthroplasty in the United States from 2005 to 2030," *J. Bone Jt. Surg. - Ser. A*, vol. 89, no. 4, pp. 780–785, 2007.
- [6] J. Raphael, M. Holodniy, S. B. Goodman, and S. C. Heilshorn, "Multifunctional coatings to simultaneously promote osseointegration and prevent infection of orthopaedic implants," *Biomaterials*, vol. 84, pp. 301–314, 2016.
- [7] Y. Li, C. Yang, H. Zhao, S. Qu, X. Li, and Y. Li, "New developments of Ti-based alloys for biomedical applications," *Materials*, vol. 7, no. 3, pp. 1709–1800, 2014.
- [8] X. Liu, P. K. Chu, and C. Ding, "Surface modification of titanium, titanium alloys, and related materials for biomedical applications," *Mater. Sci. Eng. R Reports*, vol. 47, no. 3–4, pp. 49–121, 2004.
- [9] D. M. Dohan Ehrenfest, P. G. Coelho, B. S. Kang, Y. T. Sul, and T. Albrektsson, "Classification of osseointegrated implant surfaces: Materials, chemistry and topography," *Trends Biotechnol.*, vol. 28, no. 4, pp. 198–206, 2010.
- [10] Q. Chen and G. A. Thouas, "Metallic implant biomaterials," *Mater. Sci. Eng. R Reports*, vol. 87, pp. 1–57, 2015.
- [11] J. Park and R. S. Lakes, *Biomaterials: An Introduction*. Springer, 2007.
- [12] D. F. Williams, "On the mechanisms of biocompatibility," *Biomaterials*, vol. 29, no. 20, pp. 2941–2953, 2008.
- [13] M. Geetha, A. K. Singh, R. Asokamani, and A. K. Gogia, "Ti based biomaterials, the ultimate choice for orthopaedic implants - A review," *Prog. Mater. Sci.*, vol. 54, no. 3, pp. 397–425, 2009.
- [14] W. Murphy, J. Black, and G. Hastings, *Handbook of Biomaterials Properties*. Springer, 2016.
- [15] S. Parithimarkalaignan and T. V. Padmanabhan, "Osseointegration: An update," *J. Indian Prosthodont. Soc.*, vol. 13, no. 1, pp. 2–6, 2013.
- [16] M. Niinomi, "Mechanical properties of biomedical titanium alloys," *Mater. Sci. Eng. A*, vol. 243, no. 1–2, pp. 231–236, 1998.
- [17] M. A.-H. Gepreel and M. Niinomi, "Biocompatibility of Ti-alloys for long-term implantation," *J. Mech. Behav. Biomed. Mater.*, vol. 20, pp. 407–415, 2013.
- [18] S. Minagar, C. C. Berndt, J. Wang, E. Ivanova, and C. Wen, "A review of the application of anodization for the fabrication of nanotubes on metal implant surfaces," *Acta Biomater.*, vol. 8, no. 8, pp. 2875–2888, 2012.

- [19] T. Campbell, C. Williams, O. Ivanova, and B. Garrett, “Could 3D printing change the world?,” 2011.
- [20] A. Bandyopadhyay and S. Bose, *Additive Manufacturing - Innovations, advances, and applications*, Taylor & F. 2016.
- [21] C. L. Ventola, “Medical applications for 3D printing: Current and projected uses,” *P&T*, vol. 39, no. 10, pp. 704–711, 2014.
- [22] A. Bandyopadhyay, S. Bose, and S. Das, “3D printing of biomaterials,” *MRS Bull.*, vol. 40, no. 2, pp. 108–114, 2015.
- [23] W. E. Frazier, “Metal additive manufacturing: A review,” *J. Mater. Eng. Perform.*, vol. 23, no. 6, pp. 1917–1928, 2014.
- [24] S. Bose, S. F. Robertson, and A. Bandyopadhyay, “Surface modification of biomaterials and biomedical devices using additive manufacturing,” *Acta Biomater.*, vol. 66, pp. 6–22, 2018.
- [25] E. Sallica-Leva, A. L. Jardini, and J. B. Fogagnolo, “Microstructure and mechanical behavior of porous Ti-6Al-4V parts obtained by selective laser melting,” *J. Mech. Behav. Biomed. Mater.*, vol. 26, pp. 98–108, 2013.
- [26] G. Pyka *et al.*, “Surface modification of Ti6Al4V open porous structures produced by additive manufacturing,” *Adv. Eng. Mater.*, vol. 14, no. 6, pp. 363–370, 2012.
- [27] D. Gu and Y. Shen, “Balling phenomena in direct laser sintering of stainless steel powder: Metallurgical mechanisms and control methods,” *Mater. Des.*, vol. 30, no. 8, pp. 2903–2910, 2009.
- [28] K. Gulati *et al.*, “Anodized 3D-printed titanium implants with dual micro- and nano-scale topography promote interaction with human osteoblasts and osteocyte-like cells,” *J. Tissue Eng. Regen. Med.*, vol. 11, no. 12, pp. 3313–3325, 2017.
- [29] S. Maher *et al.*, “3D printed titanium implants with nano-engineered surface titania nanotubes for localized drug delivery,” in *Chemeca 2016*, 2016.
- [30] A. Chug, S. Shukla, L. Mahesh, and S. Jadwani, “Osseointegration-Molecular events at the bone-implant interface: A review,” *J. Oral Maxillofac. Surgery, Med. Pathol.*, vol. 25, no. 1, pp. 1–4, 2013.
- [31] R. A. Gittens, R. Olivares-Navarrete, Z. Schwartz, and B. D. Boyan, “Implant osseointegration and the role of microroughness and nanostructures: Lessons for spine implants,” *Acta Biomater.*, vol. 10, no. 8, pp. 3363–3371, 2014.
- [32] T. Albrektsson and A. Wennerberg, “Oral implant surfaces: Part 1 - Review focusing on topographic and chemical properties of different surfaces and in vivo responses to them,” *Int. J. Prosthodont.*, vol. 17, no. 5, pp. 536–543, 2004.
- [33] G. Mendonça, D. B. S. Mendonça, F. J. L. Aragão, and L. F. Cooper, “Advancing dental implant surface technology - From micron- to nanotopography,” *Biomaterials*, vol. 29, no. 28, pp. 3822–3835, 2008.
- [34] E. Martínez, E. Engel, J. A. Planell, and J. Samitier, “Effects of artificial micro- and nano-structured surfaces on cell behaviour,” *Ann. Anat.*, vol. 191, no. 1, pp. 126–135, 2009.
- [35] S. Bauer, P. Schmuki, K. von der Mark, and J. Park, “Engineering biocompatible implant surfaces. Part I: Materials and surfaces,” *Prog. Mater. Sci.*, vol. 58, no. 3, pp. 261–326, 2012.

- [36] S. Hansson and M. Norton, "The relation between surface roughness and interfacial shear strength for bone-anchored implants. A mathematical model," *J. Biomech.*, vol. 32, pp. 829–836, 1999.
- [37] J. Davies, "Understanding peri-implant endosseous healing," *J. Dent. Educ.*, vol. 67, no. 8, pp. 932–949, 2003.
- [38] T. Albrektsson and C. Johansson, "Osteoinduction, osteoconduction and osseointegration," *Eur. Spine J.*, vol. 10, pp. S96–S101, 2001.
- [39] G. J. Tortora and B. Derrickson, *Principles of anatomy and physiology*. John Wiley & Sons.
- [40] M. M. Stevens, J. H. George, M. M. S. J. H. George, and J. H. G. Molly M. Stevens, "Exploring and engineering the cell surface interface," *Science*, vol. 310, no. 5751, pp. 1135–1138, 2005.
- [41] R. Brånemark, L. Emanuelsson, A. Palmquist, and P. Thomsen, "Bone response to laser-induced micro- and nano-size titanium surface features," *Nanomedicine Nanotechnology, Biol. Med.*, vol. 7, no. 2, pp. 220–227, 2011.
- [42] L. Sun, C. C. Berndt, K. A. Gross, and A. Kucuk, "Material fundamentals and clinical performance of plasma-sprayed hydroxyapatite coatings: A review," *J. Biomed. Mater. Res.*, vol. 58, no. 5, pp. 570–592, 2001.
- [43] D. Losic, M. S. Aw, A. Santos, K. Gulati, and M. Bariana, "Titania nanotube arrays for local drug delivery: recent advances and perspectives," *Expert Opin. Drug Deliv.*, vol. 12, no. 1, pp. 103–127, 2015.
- [44] D. Khudhair *et al.*, "Anodization parameters influencing the morphology and electrical properties of TiO₂ nanotubes for living cell interfacing and investigations," *Mater. Sci. Eng. C*, vol. 59, pp. 1125–1142, 2016.
- [45] S. Rani *et al.*, "Synthesis and applications of electrochemically self-assembled titania nanotube arrays," *Phys. Chem. Chem. Phys.*, vol. 12, no. 12, p. 2780, 2010.
- [46] J. M. Macak and P. Schmuki, "Anodic growth of self-organized anodic TiO₂ nanotubes in viscous electrolytes," *Electrochim. Acta*, vol. 52, no. 3, pp. 1258–1264, 2006.
- [47] J. Wan, X. Yan, J. Ding, M. Wang, and K. Hu, "Self-organized highly ordered TiO₂ nanotubes in organic aqueous system," *Mater. Charact.*, vol. 60, no. 12, pp. 1534–1540, 2009.
- [48] N. K. Awad, S. L. Edwards, and Y. S. Morsi, "A review of TiO₂ NTs on Ti metal: Electrochemical synthesis, functionalization and potential use as bone implants," *Mater. Sci. Eng. C*, vol. 76, pp. 1401–1412, 2017.
- [49] T. Kumeria *et al.*, "Advanced biopolymer-coated drug-releasing titania nanotubes (TNTs) implants with simultaneously enhanced osteoblast adhesion and antibacterial properties," *Colloids Surfaces B Biointerfaces*, vol. 130, pp. 255–263, 2015.
- [50] Y. Wang, C. Wen, P. Hodgson, and Y. Li, "Biocompatibility of TiO₂ nanotubes with different topographies," *J. Biomed. Mater. Res. - Part A*, vol. 102, no. 3, pp. 743–751, 2014.
- [51] W. Q. Yu, Y. L. Zhang, X. Q. Jiang, and F. Q. Zhang, "In vitro behavior of MC3T3-E1 preosteoblast with different annealing temperature titania nanotubes," *Oral Dis.*, vol. 16, no. 7, pp. 624–630, 2010.
- [52] P. Roy, S. Berger, and P. Schmuki, "TiO₂ nanotubes: Synthesis and applications," *Angew. Chemie - Int. Ed.*, vol. 50, no. 13, pp. 2904–2939, 2011.

- [53] J. I. Goldstein, D. E. Newbury, J. R. Michael, N. W. M. Ritchie, J. H. J. Scott, and D. C. Joy, *Scanning electron microscopy and x-ray microanalysis*, Springer. 2018.
- [54] R. Danzl, F. Helml, and S. Scherer, "Focus variation - A robust technology for high resolution optical 3D surface metrology," *Stroj. Vestn. - J. Mech. Eng.*, vol. 57, no. 3, pp. 245–256, 2011.
- [55] Q. Gui *et al.*, "Efficient suppression of nanograss during porous anodic TiO₂ nanotubes growth," *Appl. Surf. Sci.*, vol. 314, pp. 505–509, 2014.
- [56] C. Zopp, S. Blümer, F. Schubert, and L. Kroll, "Processing of a metastable titanium alloy (Ti-5553) by selective laser melting," *Ain Shams Eng. J.*, vol. 8, no. 3, pp. 475–479, 2017.
- [57] K. C. Popat, L. Leoni, C. A. Grimes, and T. A. Desai, "Influence of engineered titania nanotubular surfaces on bone cells," *Biomaterials*, vol. 28, no. 21, pp. 3188–3197, 2007.
- [58] J. Park, S. Bauer, K. Von Der Mark, and P. Schmuki, "Nanosize and vitality: TiO₂ nanotube diameter directs cell fate," *Nano Lett.*, vol. 7, no. 6, pp. 1686–1691, 2007.
- [59] K. Gulati, A. Santos, D. Findlay, and D. Losic, "Optimizing anodization conditions for the growth of titania nanotubes on curved surfaces," *J. Phys. Chem. C*, vol. 119, no. 28, pp. 16033–16045, 2015.
- [60] E. Balaur, J. M. MacAk, L. Taveira, and P. Schmuki, "Tailoring the wettability of TiO₂ nanotube layers," *Electrochem. commun.*, vol. 7, no. 10, pp. 1066–1070, 2005.
- [61] F. Rupp *et al.*, "A review on the wettability of dental implant surfaces I: Theoretical and experimental aspects," *Acta Biomater.*, vol. 10, no. 7, pp. 2894–2906, 2014.
- [62] S. Oh, C. Daraio, L.-H. Chen, T. R. Pisanic, R. R. Finões, and S. Jin, "Significantly accelerated osteoblast cell growth on aligned TiO₂ nanotubes," *Journal Biomed. Mater. Res. Part A*, vol. 78A, no. 1, pp. 97–103, 2006.
- [63] O. K. Varghese, D. Gong, M. Paulose, C. A. Grimes, and E. C. Dickey, "Crystallization and high-temperature structured stability of titanium oxide nanotube arrays," *J. Mater. Res.*, vol. 18, no. 1, pp. 156–165, 2003.
- [64] T. Kokubo and H. Takadama, "How useful is SBF in predicting in vivo bone bioactivity?," *Biomaterials*, vol. 27, no. 15, pp. 2907–2915, 2006.
- [65] L. Mohan, C. Anandan, and N. Rajendran, "Electrochemical behaviour and bioactivity of self-organized TiO₂ nanotube arrays on Ti-6Al-4V in Hanks' solution for biomedical applications," *Electrochim. Acta*, vol. 155, pp. 411–420, 2015.
- [66] K. Gulati, M. S. Aw, D. Findlay, and D. Losic, "Local drug delivery to the bone by drug-releasing implants: perspectives of nano-engineered titania nanotube arrays," *Ther. Deliv.*, vol. 3, no. 7, pp. 857–73, 2012.